RESEARCH ARTICLE

Tripartite interactions of PKA catalytic subunit and C-terminal domains of cardiac Ca^{2+} channel may modulate its β-adrenergic regulation

Shimrit Oz[1,2], Tal Keren-Raifman[1], Tom Sharon[1], Suraj Subramaniam[3], Tamara Pallien[4], Moshe Katz[1], Vladimir Tsemakhovich[1], Anastasiia Sholokh[4], Baraa Watad[1], Debi Ranjan Tripathy[1,3,9], Giorgia Sasson[3], Orna Chomsky-Hecht[3], Leonid Vysochek[5], Maike Schulz-Christian[4], Claudia Fecher-Trost[6], Kerstin Zühlke[4], Daniela Bertinetti[7], Friedrich W. Herberg[7], Veit Flockerzi[6], Joel A. Hirsch[3], Enno Klussmann[4,8], Sharon Weiss[1]* and Nathan Dascal[1]*

Abstract

Background The β-adrenergic augmentation of cardiac contraction, by increasing the conductivity of L-type voltage-gated Ca$_V$1.2 channels, is of great physiological and pathophysiological importance. Stimulation of β-adrenergic receptors (βAR) activates protein kinase A (PKA) through separation of regulatory (PKAR) from catalytic (PKAC) subunits. Free PKAC phosphorylates the inhibitory protein Rad, leading to increased Ca^{2+} influx. In cardiomyocytes, the core subunit of Ca$_V$1.2, Ca$_V$1.2α$_1$, exists in two forms: full-length or truncated (lacking the distal C-terminus (dCT)). Signaling efficiency is believed to emanate from protein interactions within multimolecular complexes, such as anchoring PKA (via PKAR) to Ca$_V$1.2α$_1$ by A-kinase anchoring proteins (AKAPs). However, AKAPs are inessential for βAR regulation of Ca$_V$1.2 in heterologous models, and their role in cardiomyocytes also remains unclear.

Results We show that PKAC interacts with Ca$_V$1.2α$_1$ in heart and a heterologous model, independently of Rad, PKAR, or AKAPs. Studies with peptide array assays and purified recombinant proteins demonstrate direct binding of PKAC to two domains in Ca$_V$1.2α$_1$-CT: the proximal and distal C-terminal regulatory domains (PCRD and DCRD), which also interact with each other. Data indicate both partial competition and possible simultaneous interaction of PCRD and DCRD with PKAC. The βAR regulation of Ca$_V$1.2α$_1$ lacking dCT (which harbors DCRD) was preserved, but subtly altered, in a heterologous model, the *Xenopus* oocyte.

Conclusions We discover direct interactions between PKAC and two domains in Ca$_V$1.2α$_1$. We propose that these tripartite interactions, if present in vivo, may participate in organizing the multimolecular signaling complex and fine-tuning the βAR effect in cardiomyocytes.

*Correspondence:
Sharon Weiss
lahavsha@tauex.tau.ac.il
Nathan Dascal
dascaln@tauex.tau.ac.il
Full list of author information is available at the end of the article

Oz *et al. BMC Biology* (2024) 22:276

Page 2 of 22

Background

Ca^{2+} influx via L-type voltage-gated Ca^{2+} channels ($Ca_V1.2$) underlies cardiac excitation–contraction coupling [1]. $Ca_V1.2$ channels are prominently modulated by epinephrine and the sympathetic nervous system, underlying much of the physiological regulation of heartbeat and the "fight-or-flight" response, via the activation of β-adrenergic receptors (βAR), β1AR and β2AR [2]. The ensuing signaling cascade leads to elevated cAMP levels, activation of protein kinase A (PKA) by the disassembly of the PKA holoenzyme into catalytic (PKAC) and regulatory (PKAR) subunits [3, 4] (Fig. 1), and culminates in the enhancement of $Ca_V1.2$ channel currents. In cardiomyocytes much of this signaling occurs within precise micro/nanodomains (signalosomes) that have been proposed to include the βARs, G proteins, adenylyl cyclase, PKA, $Ca_V1.2$, and additional interacting proteins [5–9]. Dysregulation of this cascade may result in heart failure and certain arrhythmias, such as catecholaminergic polymorphic ventricular tachycardia (CPVT) [10]. β1ARs are located mostly at the crest and signal globally; β2ARs interact and co-localize with $Ca_V1.2$ at the t-tubules, and signal locally [5, 11–15]. Despite decades of intense research [16], crucial aspects of this regulation, such as the spatiotemporal organization of the signaling complexes and the target(s) of PKA phosphorylation, remain unclear or debatable [17–19]. Here we report a novel direct interaction of PKAC with two regulatory segments of $Ca_V1.2$, PCRD, and DCRD. We propose that these interactions may modulate the βAR-$Ca_V1.2$ signaling, partly by driving colocalization of PKA with $Ca_V1.2$ within the macromolecular signaling complex.

$Ca_V1.2$ channels comprise the pore-forming subunit $Ca_V1.2\alpha_1$ (also termed α_{1C}), intracellular $Ca_V\beta$ and
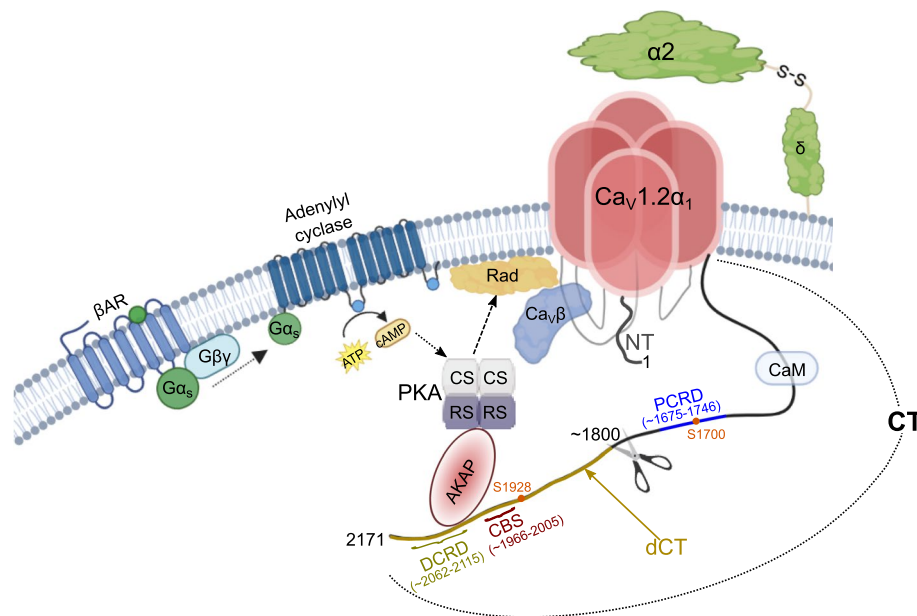

Fig. 1 The current concept of the signaling pathway underlying the β-adrenergic regulation of $Ca_V1.2$ in cardiomyocytes. The cascade is initiated by the binding of an agonist (e.g., epinephrine or norepinephrine; depicted as a small green circle) to a β-adrenergic receptor (βAR) which, in turn, activates the G protein G_s by catalyzing GDP-GTP exchange at the $G\alpha_s$ subunit followed by separation of the latter from the $G\beta\gamma$ subunit. The GTP-bound $G\alpha_s$, alone or in concert with $G\beta\gamma$, activates adenylyl cyclase (AC), promoting the conversion of ATP to cAMP. cAMP activates PKA, causing the dissociation of its regulatory (RS) from catalytic (CS) subunits. CS phosphorylates several targets including $Ca_V1.2\alpha_1$ and $Ca_V\beta$ subunits, but the most important target in $Ca_V1.2$ regulation appears to be the Rad protein. Phosphorylation of Rad removes the constitutive inhibition that it exerts upon channel activity, through separation of Rad from $Ca_V\beta$. According to the classical prevalent scheme: before activation, the PKA holoenzyme is associated with the $Ca_V1.2\alpha_1$ subunit via an AKAP protein that strongly binds PKAR (the binding main sites for most AKAPs are in the dCT of $Ca_V1.2\alpha_1$); however, as detailed in the text, AKAPs are probably not strictly required in cardiomyocytes. The scheme also shows the auxiliary subunits of $Ca_V1.2$ and the cytosolic domain of $Ca_V1.2\alpha_1$: N-terminus (NT), C-terminus (CT) (with dCT colored dark mustard), and intracellular loops (shown in light gray). Also indicated are the approximate CT proteolytic cleavage site (scissors), major PKA phosphorylation sites in the CT (S1700 and S1928), and the DCRD, CBS, and PCRD domains

Oz et al. BMC Biology   (2024) 22:276

Page 3 of 22

calmodulin (CaM), and extracellular α2δ [20–22]. Much of the cardiac $Ca_V1.2\alpha_1$ is post-translationally cleaved at the C-terminus (CT), around amino acid (a.a.) 1800–1820, to produce the truncated $Ca_V1.2\alpha_1$ protein and the cleaved distal CT ($Ca_V1.2\alpha_1$-dCT) [23–26] (Fig. 1); however, full-length (FL) $Ca_V1.2\alpha_1$ protein is also present [24, 25, 27]. The ratio of truncated/full-length channels in cardiomyocytes has not been definitely quantified and remains a controversy [17, 27]; it may be species, organ, and age-dependent [23, 28, 29]. The specific protease that cleaves $Ca_V1.2\alpha_1$ in cardiomyocytes is unknown; in neurons, the dCT cleavage is Ca^{2+}-dependent and catalyzed by calpain [30].

The $Ca_V1.2\alpha_1$-dCT is an important regulator of $Ca_V1.2$. In the full-length channel, it acts as an inhibitory module that reduces the channel's open probability and voltage sensitivity [31, 32]. It has been suggested that the autoinhibition of $Ca_V1.2$ function by the $Ca_V1.2\alpha_1$-dCT domain plays a role in PKA regulation [2, 33, 34] but the mechanism and extent of such regulation remain unclear. $Ca_V1.2\alpha_1$-dCT also serves as a binding hub for signaling proteins, such as the protein phosphatase PP2A, several A-kinase anchoring proteins (AKAPs), β2AR, and others [15, 27, 35–38], and was suggested to take part in PKA regulation of the channel [2, 24, 39]. An unknown fraction of the cleaved $Ca_V1.2\alpha_1$-dCT translocates to the nucleus and acts as a transcription regulator for $Ca_V1.2$ and other proteins [40, 41], and a fraction was also proposed to remain bound to, and inhibit, the truncated channel [24].

Two separate regulatory domains within $Ca_V1.2\alpha_1$-CT were previously identified [24]: one proximal to the truncation (PCRD: Proximal C-terminus Regulatory Domain; a.a. 1675–1746) and the other one distal to the truncation (DCRD: Distal C-terminus Regulatory Domain) (Fig. 1). The DCRD takes part in dCT-induced inhibition of the channel, probably due to its interaction with PCRD [24]. Interestingly, proximally to DCRD, a novel $Ca_V\beta$-binding site in the $Ca_V1.2\alpha_1$-dCT, termed C-terminal β-Binding Site (CBS), has been recently identified [42] (Fig. 1).

Spatial and functional organization of βAR/PKA/$Ca_V1.2$ signaling involves AKAPs, scaffolding proteins orchestrating the assembly of cell compartment-specific macromolecular complexes [27, 43–48]. In a classical scheme, the PKA holoenzyme is docked to $Ca_V1.2\alpha_1$-dCT indirectly, via an AKAP that possesses separate binding sites for PKAR and $Ca_V1.2\alpha_1$-dCT and the plasma membrane (Fig. 1). Binding of cAMP to PKAR releases PKAC from PKAR, enabling the PKAC to phosphorylate the target protein [38, 49–51]. However, it is unclear how important AKAPs are for the βAR regulation of cardiac $Ca_V1.2$. Initial reports suggested a central role of AKAP5 (AKAP79/150) or

AKAP7 (AKAP15/18) [50, 51], yet, genetic ablation of AKAP5 and AKAP7 did not significantly attenuate the βAR upregulation of $Ca_V1.2$ in cardiomyocytes [52, 53]. Deletion of another AKAP, Cypher/ZASP, weakened the regulation [37, 54]. Moreover, the presence of dCT that contains the main binding site for most AKAPs is not essential for PKA regulation, since heterologously expressed $Ca_V1.2$, either full-length or dCT-truncated, is robustly regulated by activation of PKA and βARs without AKAP coexpression [55, 56]. Thus, while AKAP anchoring of PKA may be crucial for $Ca_V1.2$ regulation in some organs [19], it does not appear essential in cardiac muscle.

Importantly, it is unclear whether full length and truncated $Ca_V1.2\alpha_1$ forms of $Ca_V1.2$ are differently regulated by βARs and PKA. The most prominent PKA phosphorylation sites in $Ca_V1.2\alpha_1$, Ser1700 and Ser 1928, are located in PCRD and in the cleaved $Ca_V1.2\alpha_1$-dCT, respectively (Fig. 1). Direct phosphorylation of one of these sites has long been believed to underlie the PKA regulation of $Ca_V1.2$ [2]. This appears to hold true for the phosphorylation of Ser1928 in neurons and smooth muscle [57–60], and it may be involved in channel oligomerization upon βAR activation [61]. However, it is not the case in the heart, as shown by studies in cellular systems and genetically engineered mice [17, 18, 25, 62–64], although a regulatory role for $Ca_V1.2\alpha_1$ phosphorylation has not been ruled out [65, 66]. Recent seminal studies [55, 67–69] identified phosphorylation of Rad as an essential step in βAR-$Ca_V1.2$ regulation in the heart (Fig. 1) and decisively demonstrated that coexpression of Rad is essential for the reconstitution of the adrenergic regulation of $Ca_V1.2$ in heterologous expression systems [55, 56]. Rad constitutively inhibits cardiac $Ca_V1.2$, mainly via an interaction with the β subunit [70–74]. PKA phosphorylation of Rad removes it from the plasma membrane, disrupts $Ca_V1.2$-Rad proximity and $Ca_V\beta$-Rad interaction, and alleviates Rad's inhibitory effect on $Ca_V1.2$ [55, 75–77].

Given the robust βAR regulation of the truncated $Ca_V1.2$ [56], lacking the key AKAP-binding sites, we hypothesized that there may be an AKAP-independent mechanism to ensure PKA proximity to $Ca_V1.2\alpha_1$ following adrenergic stimulation. We found that PKAC co-precipitates with dCT-truncated $Ca_V1.2\alpha_1$ ($Ca_V1.2\alpha_{1\Delta1821}$), independently of PKAR. We then mapped the interaction sites to both PCRD and DCRD and demonstrated their direct interaction with PKAC and with each other. Our results suggest unique interaction sites for PKAC on $Ca_V1.2\alpha_1$-PCRD, present in both FL and truncated channels, and in the dCT (only in FL channels). These intricate, AKAP-independent interactions likely regulate the efficacy of the signaling cascade.

Oz et al. BMC Biology   (2024) 22:276

Page 4 of 22

Results

Protein kinase A catalytic subunit and $Ca_V1.2\alpha_{1\Delta1821}$ co-immunoprecipitate independently of PKA-regulatory subunit

To examine the possibility that PKA interacts directly with a truncated $Ca_V1.2\alpha_1$ lacking the AKAP-binding $Ca_V1.2\alpha_1$-dCT, we have generated a HEK293 cell line stably expressing tetracycline-inducible mouse $Ca_V1.2\alpha_{1\Delta1821}$ (Additional File 1: Fig. S1A, B [9, 29, 56, 78–81]). As shown previously in these cells [82] and HEK293-derived TsA201 cells [83], we observed that these cells also express endogenous $Ca_V\beta$ subunits (Additional File 1: Fig. S1C), which most likely contribute to the formation of functional channels. Tetracycline-induced expression of $Ca_V1.2\alpha_{1\Delta1821}$ resulted in typical calcium channel currents that were significantly enhanced by coexpression of the auxiliary subunits, $Ca_V\beta_2$ and $\alpha2\delta1$ (Additional File 1: Fig. S1D,E). Next, we transiently transfected the $Ca_V1.2\alpha_{1\Delta1821}$ HEK293 cells with YFP-fused

PKAC (PKAC-YFP) and performed immunoprecipitation (IP) of $Ca_V1.2\alpha_1$ (Fig. 2A). IP with the $Ca_V1.2\alpha_1$ antibody, but not $Na_V1.1$ sodium channel antibody, specifically precipitated $Ca_V1.2\alpha_{1\Delta1821}$. Importantly, we observed co-immunoprecipitation (co-IP) of PKAC-YFP with $Ca_V1.2\alpha_{1\Delta1821}$. PKAC-YFP was detected by the PKAC antibody at ~70 kDa only in cells that expressed both $Ca_V1.2\alpha_{1\Delta1821}$ and PKAC-YFP and when the IP was done with the $Ca_V1.2\alpha_1$ antibody, but not in the control IP with the $Na_V1.1$ antibody (Fig. 2A, right panel).

In a complementary experiment (Fig. 2B), transiently expressed PKAC-YFP (precipitated with the GFP antibody) co-precipitated $Ca_V1.2\alpha_{1\Delta1821}$ and the transiently expressed HA-tagged PKA-regulatory subunit (PKAR-HA, detected with anti-HA antibody). PKA activators (forskolin and/or cAMP) considerably decreased the amount of PKAR co-precipitated with PKAC, as expected. In contrast, the amount of co-precipitated $Ca_V1.2\alpha_{1\Delta1821}$ did not decrease following this treatment
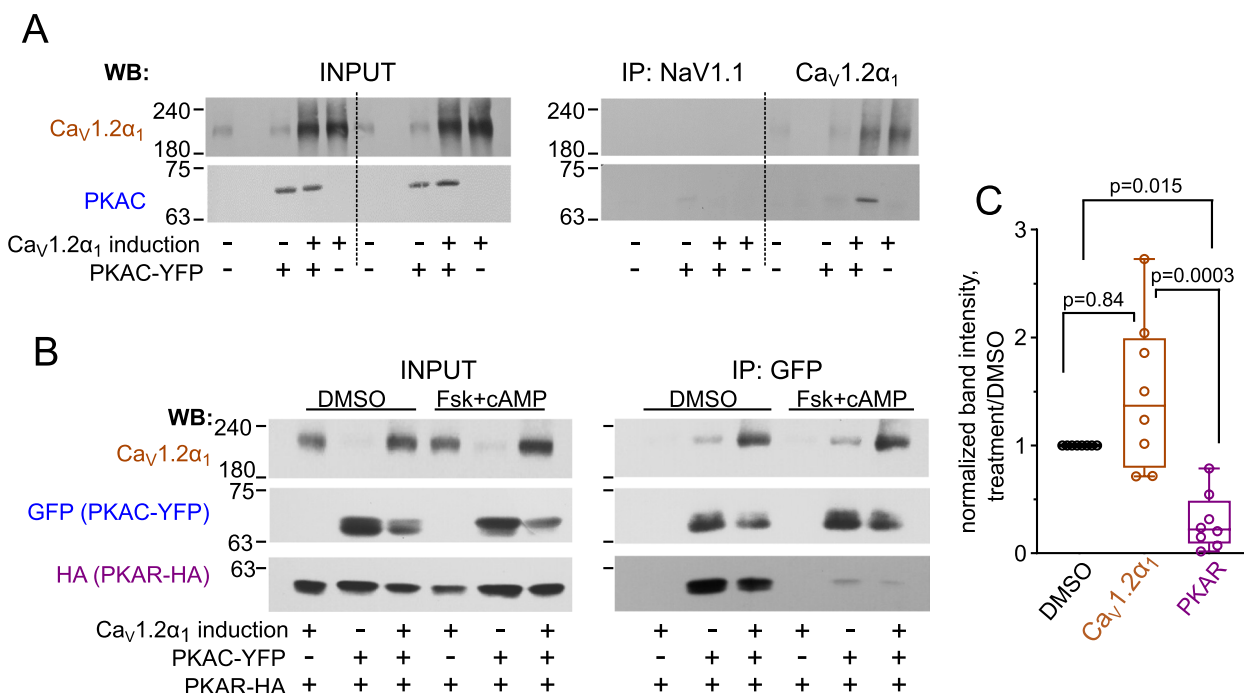

Fig. 2 $Ca_V1.2\alpha_{1\Delta1821}$ and PKAC co-immunoprecipitate independently of PKAR. **A** *left panel:* Tetracycline administration induced $Ca_V1.2\alpha_{1\Delta1821}$ expression in HEK293 cells stably transfected with $Ca_V1.2\alpha_{1\Delta1821}$, with or without transiently expressed PKAC-YFP (marked as input). *Right panel*: $Ca_V1.2\alpha_1$ antibody, but not sodium channel subunit antibody, $Na_V1.1$, specifically enriched $Ca_V1.2\alpha_{1\Delta1821}$ and co-precipitated transiently expressed PKAC-YFP (detected by PKAC antibody) only in cells that co-express $Ca_V1.2\alpha_{1\Delta1821}$ and PKAC-YFP. Note that in Tet-conditional stable cell lines, in the absence of tetracycline the promoter activity is minimal but often shows some basal activity [84], as revealed by the faint band of $Ca_V1.2\alpha_1$, visible by IP. **B** *left panel:* Tetracycline administration induced $Ca_V1.2\alpha_1$ expression, with or without transiently expressed PKAC-YFP and PKAR-HA (marked as input). *Right panel*: GFP antibody specifically enriched PKAC-YFP and co-precipitated $Ca_V1.2\alpha_{1\Delta1821}$ and PKAR-HA. Addition of forskolin and cAMP, but not DMSO, lowered the amount of co-precipitated PKAR, but did not affect co-precipitated $Ca_V1.2\alpha_{1\Delta1821}$. **C** PKA activators enhanced the interaction of PKAC with $Ca_V1.2\alpha_{1\Delta1821}$ (1.47 ± 0.25, $n = 8$) and reduced its interaction with PKAR (0.29 ± 0.09, $n = 8$) relative to control (without PKA activators, with DMSO only). Y axis shows normalized band intensity relative to control. Statistics: Kruskal–Wallis test followed by Dunn's multiple comparison test (p values are shown for all comparisons). A separate statistical analysis using one-sample t-test vs. DMSO control confirmed that the change in binding to $Ca_V1.2\alpha_{1\Delta1821}$ was not statistically significant for PKAC ($p = 0.097$) but significant for PKAR ($p = 0.015$)

Oz et al. BMC Biology   (2024) 22:276

Page 5 of 22

(Fig. 2B, right panel). Overall, PKA activation by forskolin and/or cAMP reduced the amount of PKAR interacting with PKAC by about 70% (0.29 ± 0.09, $n = 8$) compared to control (Fig. 2C), and did not reduce the amount of PKAC-interacting $Ca_V1.2\alpha_{1\Delta1821}$ (the slight increase, 1.47 ± 0.25, $n = 8$, did not reach statistical significance). Taken together, these results suggest that PKAC directly interacts with $Ca_V1.2\alpha_{1\Delta1821}$, independently of its interaction with PKAR or the presence of $Ca_V1.2\alpha_1$-dCT, and does not require coexpression of either Rad or AKAPs.

We further examined whether endogenous PKAC can be co-immunoprecipitated with $Ca_V1.2\alpha_1$ from the left ventricle of rat heart (Additional File 1: Fig. S2; Additional File 2). We used 4–20% gradient or 7.5% gels to be able to visualize both $Ca_V1.2\alpha_1$ and PKAC, which made it technically difficult to separate full-length $Ca_V1.2\alpha_1$ from its truncated form [29]; nevertheless, it is clear from Fig. S2 that the $Ca_V1.2\alpha_1$ antibody precipitated both $Ca_V1.2\alpha_1$ and PKAC.

Mapping PKAC and $Ca_V1.2\alpha_1$-CT interaction sites

We used scanning peptide array analysis, suitable for mapping sites of interaction in proteins, to identify interaction sites in $Ca_V1.2\alpha_1$ and PKAC. Since the initial part of the NT and residues within the CT, but not the cytosolic loops 1–3 connecting the channel's repeating domains, have been implicated in PKA regulation of $Ca_V1.2$ [34, 51, 57, 60, 85], we prepared an array of 25-mer spot-immobilized overlapping peptides covering the first half of human and rabbit NT and the whole CT domain of rabbit $Ca_V1.2\alpha_1$, excluding the specific calmodulin-binding IQ motif. (Rabbit $Ca_V1.2\alpha_1$ was the model channel used in this and most previous studies, and it is robustly regulated by PKA in heterologous reconstitution systems [55, 56, 67]). We overlaid the membrane with purified His-PKAC protein and probed it with PKAC antibody (Additional File 1: Fig. S3). We detected moderate binding to the initial 25 a.a. of the human NT; this binding was enhanced by alanine mutations of most a.a. residues in this peptide (Additional File 1: Fig. S3, spot E16). However, no significant PKAC binding was detected in the initial 25 a.a. segment of NT of the rabbit $Ca_V1.2\alpha_1$ (three a.a. difference from the same segment of human $Ca_V1.2\alpha_1$ NT), or in the rest of the NT (100% identity with the human NT).

In contrast to the N-terminus, we reproducibly observed strong interaction (black spots) of PKAC with three domains in $Ca_V1.2\alpha_1$-CT: K1672-G1731, V1737-E1776 and L2072-L2126 (Fig. 3A, B; Additional File 1: Fig. S3). Interestingly, the two main interaction domains partially overlap PCRD (Q1675 -S1746) and DCRD (S2062—G2115), the two domains previously proposed to interact with each other, underlying the auto-inhibitory action of the dCT [24]. Notably, PCRD contains the PKA recognition sequence $^{1696}RRxxS^{1700}$
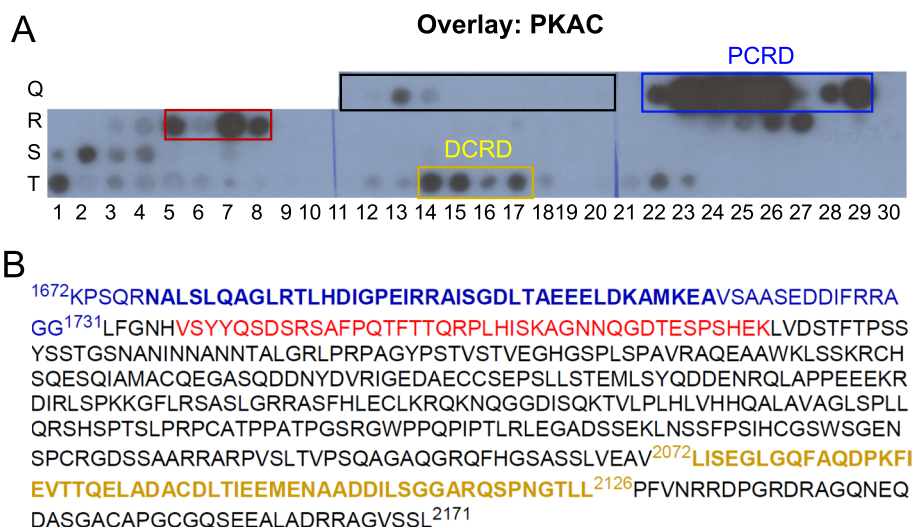

Fig. 3 Peptide array reveals PKAC interaction sites within $Ca_V1.2\alpha_1$ -CT. **A** An array of 25-mer overlapping peptides with a 5 a.a. shift from $Ca_V1.2\alpha_1$-CT segment, immobilized as spots on a membrane, were overlaid with purified His-PKAC and probed with PKAC antibody. Shown is the part of the membrane presenting the CT region between a.a. 1576–1647 (framed in black box) and a.a. 1672–2171 (the rest of the array). Within this segment, cysteines were replaced with serines to avoid the formation of disulfide bridges. See Additional File 1: Fig. S3 for the image of the full array and additional details. The overlay reveals three main interaction domains on $Ca_V1.2\alpha_1$-CT: K1672-G1731 (PCRD; framed in blue box), V1737-E1776 (red box) and L2072-L2126 (DCRD; dark yellow box). Shown are representative results of four independent experiments. **B** Amino acid sequence of the interaction domains; color code same as boxes in **A**

Oz *et al. BMC Biology*　　(2024) 22:276

Page 6 of 22

with the well characterized PKA phosphorylation site S^{1700} [2].

For further study of the interaction between PKAC and PCRD or DCRD segments of $Ca_V1.2\alpha_1$ by rigorous biochemical and biophysical methods, we prepared purified recombinant PCRD (G1671-T1751) and DCRD (R2058-S2120) proteins. We prepared DNA constructs for bacterial expression of His-DCRD, His-DRCD-Myc, and His-SUMO-PCRD. (SUMO protein was fused to PCRD to improve expression and stability of the protein). Both proteins were expressed in *E. coli* and purified. His-DCRD-Myc (DCRD in brief) showed a strong protein band of the predicted molecular mass (11.5 KDa; Additional File 1: Fig. S4). The purified His-SUMO-PCRD appeared in two distinct molecular sizes that were detected by the SUMO antibody, indicating that the protein is partially truncated at its C-terminus. The full-length ~ 25 kDa protein ("peak 2", Additional File 1: Fig. S5 A-C) tended to degrade during the experiment. The major protein fraction ("peak 3", Additional File 1: Fig. S5 A-C) contained a single main protein product running at ~ 17 kDa, as shown by SDS PAGE and HPLC analysis (Additional File 1: Fig. S5D). We have termed this protein His-SUMO-PCRD$_{trunc}$, or PCRD$_{trunc}$ for brevity. Further analysis of PCRD$_{trunc}$ by mass spectrometry (Additional File 1: Fig. S5E) confirmed that it extends to Y^{1739} and thus includes the main putative PKAC-binding, PCRD-overlapping segment detected in the peptide array (Fig. 3). It also contains the aforementioned PKA recognition sequence that is expected to bind PKAC. Importantly, this segment in PCRD is homologous to known PKA-binding pseudosubstrate sites found in PKAR and the specific PKA inhibitor, PKI (Additional File 1: Fig. S5F) [86, 87]. The peptide array indicates a smaller putative PKAC binding site downstream from PCRD$_{trunc}$ (labeled by red frame in Fig. 3A and red letters in Fig. 3B); we have not further studied this putative interaction site.

To further characterize the interaction between PKAC and PCRD or DCRD and to map the sites of interaction in PKAC, we next scanned an array of 25-mer overlapping peptides covering the full-length of PKAC, using overlays with DCRD (detected by Myc antibody) or PCRD$_{trunc}$ (detected by His antibody). The overlay experiments suggested two surfaces on PKAC that interact with PCRD. One of these also interacted with DCRD, but appeared more extended than the DCRD site (Fig. 4C). The binding sites partially overlap with RyR2 binding sites on PKAC [88]. The array results also indicated possible additional shorter DCRD-binding segments, but they were not consistent between replicates. Overall, these results strengthen the notion that PKAC directly interacts with PCRD and DCRD.

PCRD and DCRD directly interact with PKAC in a concentration-dependent manner

To further corroborate the direct interaction between PKAC and the PCRD and DCRD domains of $Ca_V1.2\alpha_1$, we used purified recombinant proteins. First, we examined the binding of GST-PKAC to His-labeled PCRD$_{trunc}$ and DCRD by pulldown on Ni–NTA beads. The results demonstrated concentration-dependent, saturable interaction of both PCRD and DCRD with PKAC (Fig. 5). Control experiments verified that purified His-SUMO alone did not bind PKAC (Additional File 1: Fig. S6). The binding data could be fitted to Hill's equation with an apparent dissociation constant below 1 µM for both proteins. Since the pulldown procedure involves multiple steps and the local concentration of proteins attached to Ni–NTA beads is unknown, the apparent sub-micromolar affinity estimates may not reflect the actual affinity.

To obtain a better estimate of the thermodynamic parameters of PKAC interaction with PCRD$_{trunc}$, we used isothermal titration calorimetry (ITC) (Fig. 6). The ITC confirmed the concentration-dependent and saturable binding between PKAC and PCRD$_{trunc}$ with a K_D of 1.4 µM. Interestingly, the estimated PCRD/PKAC molar ratio was 1.73, supporting the possibility of two PCRD binding sites in PKAC as suggested by the peptide array scan (Fig. 4).

Tripartite interaction between PKAC, PCRD, and DCRD

PCRD and DCRD have been proposed to interact, presumably by forming salt bridges between R1696/R1697 (PCRD) and E2103/E2106/D2110 (DCRD) [24]. Using synthetic fluorescein-labeled, 30- or 44-mer peptides, PCRD30 and PCRD44 (Fig. 7A), we found that purified recombinant His-PKAC, but not PKAR (we used PKA-RII), bound the PCRD30 and PCRD44 peptides in a pulldown assay (Fig. 7B). The extent of binding to PKAC was similar for PCRD30 and PCRD44, suggesting that the distal part of PCRD44 (the last 14 a.a.) is not crucial for this interaction. Moreover, His-DCRD also bound PCRD30 and PCRD44.

The confirmation of direct interaction between DCRD and PCRD, both of which bind PKAC at the same ~ 30-a.a. segment (see Fig. 4), raised the possibility of competition between PCRD and DCRD for binding to PKAC. We examined the binding between GST-PKAC and PCRD30 in the presence of increasing concentrations of His-DCRD. GST-PKA-RII served as a negative control. Addition of DCRD resulted in decreased binding between PKAC and PCRD30, with half-inhibition concentration (IC$_{50}$) of 0.88 µM (Fig. 7C, D). DCRD did not cause a complete dissociation of PCRD30 from PKAC, leaving a significant PKAC-bound fraction of PCRD30 peptide (~ 25% at saturating DCRD concentrations, as
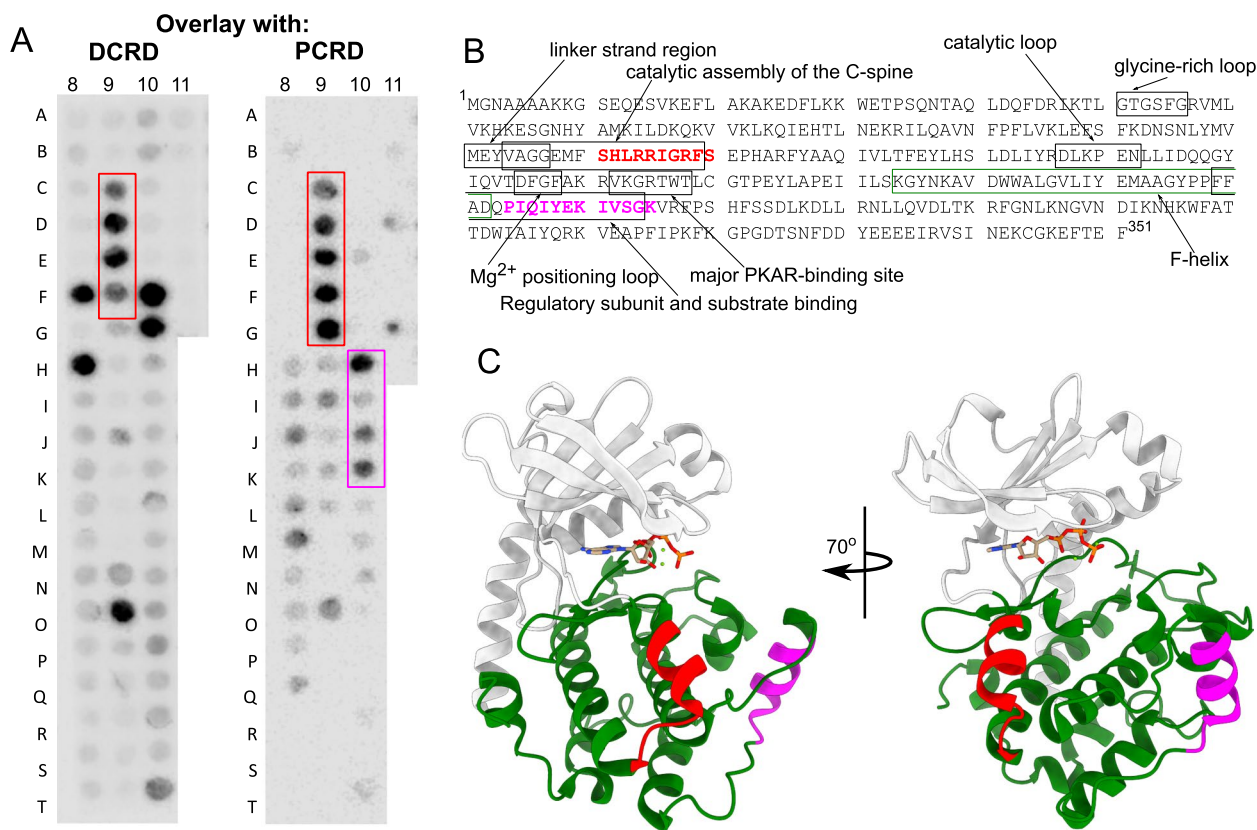
Oz et al. BMC Biology   (2024) 22:276

Page 7 of 22

Fig. 4 Peptide array reveals interaction sites of PCRD and DCRD with PKAC. **A** An array of 25-mer overlapping peptides, with a 5 a.a. shift, of PKAC immobilized as spots on a membrane were overlaid with purified His-DCRD-Myc (left) and His-SUMO-PCRD (right). The overlay reveals a common DCRD/PCRD binding site (framed in red) and an additional PCRD unique site (magenta) on PKAC. Shown are representative results of three independent experiments. **B** PCRD and DCRD binding sites on PKAC are located within solvent exposed helices. **C** Side view (left) and a 70° rotated view (right) cartoons of human PKAC protein (PDB: 4WB5 [89]). The PKI peptide and amino acids 311–350 of this structure were removed for clarity. An ATP molecule with 2 metal ions is depicted as sticks in the catalytic site. The PKAC N-terminal domain is colored gray, the C-terminal domain green, the common PCRD/DCRD binding site red, and the unique PCRD binding site magenta

estimated from the results of fitting of the binding curve; Fig. 7D). This indicates that a fraction of PCRD30 present in the reaction may remain bound to PKAC in the presence of excess DCRD, or that more than one conformation of PCRD-PKAC complex exist, so that it may be inaccessible to DCRD. In a complementary experiment, increasing doses of the PCRD30 peptide did not significantly affect the binding between His-DCRD and GST-PKAC (Additional File 1: Fig. S7). The latter result may indicate that the affinity of this peptide to PKAC, at the common PCRD/DCRD site, may be low compared to DCRD. Taken together, the results so far suggest a tripartite interaction between PKAC, PCRD, and DCRD in which the three partners bind each other and may potentially form a triple complex.

To address the potential functional consequences of the tripartite PKA-PCRD-DRCD interactions, we first tested the hypothesis that the interaction with PCRD or DCRD may affect the catalytic activity of PKAC. We examined the effect of purified PCRD$_{trunc}$ and DCRD on PKAC catalytic activity using two different assays with standard PKA substrates. Neither PCRD$_{trunc}$ nor DCRD caused any significant changes in PKAC activity (Additional File 1: Fig. S8).

Differences in β1AR modulation of full-length and truncated Ca$_V$1.2 channels

As discussed above, in cardiomyocytes the two forms of Ca$_V$1.2α$_1$ coexist in an unknown proportion, and it is not known if they are distinctly regulated by PKA. A difference may be expected in light of our discovery of the tripartite interaction between PKAC and proximal and distal parts of Ca$_V$1.2α$_1$ C-terminus. Therefore, we assessed the role of Ca$_V$1.2α$_1$-dCT and the proteolytic processing of cardiac Ca$_V$1.2α$_1$ using a functional electrophysiological assay. We compared the β1AR regulation of Ca$_V$1.2 containing either FL or truncated Ca$_V$1.2α$_1$ in a heterologous expression system. To date,
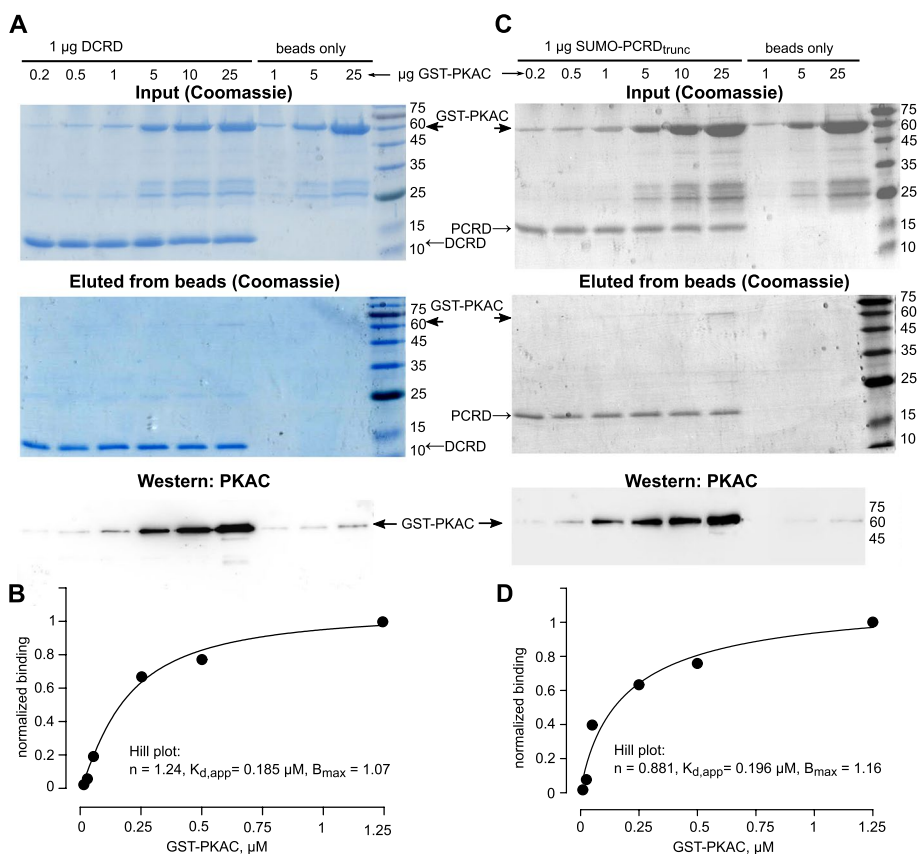
A

C

B

D

Fig. 5 Dose dependent binding of GST-PKAC to DCRD and PCRD_trunc. One microgram of purified DCRD (**A**, **B**) or PCRD_trunc (**C**, **D**) was used to pull down the indicated amounts of GST-PKAC on Ni–NTA beads. The reaction volume was 300 µl. **A** DCRD/PKAC interaction. Upper gel: input (Coomassie staining of a separate gel with exactly the same amounts of proteins as for pull-down reaction shown in the middle gel). Middle gel: elution from beads (Coomassie). Lower image: Western blot of the eluted proteins, with PKAC antibody. **B** Quantitation of the binding curve for the DCRD-PKAC experiment. Data were analyzed with ImageJ. Intensities of GST-PKAC binding were normalized to 25 µg GST-PKAC (lane 6). Data were fitted to a Hill equation in the form $f = B_{max} * [PKA]^n / ([PKA]^n + K_{d,app}{}^n)$, where B_{max} is maximal binding, [PKA] is GST-PKAC concentration, $K_{d,app}$ is the apparent dissociation coefficient, and n is Hill coefficient. The parameters of the fit are shown in the inset. Representative of 4 experiments. **C** PCRD_trunc/PKAC interaction (same presentation as in **A**). Upper gel: input (Coomassie); middle gel: elution from beads (Coomassie); lower image: Western blot of the eluted proteins, with PKA antibody. **D** Quantitation of the binding curve for the PCRD_trunc-PKAC experiment. Representative of 3 experiments

Xenopus oocyte is the only model cell in which the full adrenergic cascade of regulation of Ca_V1.2 (starting with the activation of the βAR) has been reconstituted. The oocytes also present the rare advantage of maintaining stable Ba²⁺ currents (I_Ba) via Ca_V1.2 (following an initial stabilization) over tens of minutes [56, 85, 90, 91], which is important for studying the relatively slow βAR regulation. In a previous study we demonstrated robust, Rad-dependent βAR regulation of both full-length and truncated Ca_V1.2 by β1AR or β2AR [56]. The regulation of I_Ba by the βAR agonist isoproterenol (Iso) appeared smaller in the case of the FL Ca_V1.2α_1 [56] but in a limited range of current amplitudes, especially for Ca_V1.2α_1-FL. We have therefore decided to

characterize the βAR regulation of the two forms of Ca_V1.2 in more detail and in a wider amplitude range.

Oocytes were injected with RNAs of all channel subunits (Ca_V1.2α_1 FL or Ca_V1.2α_{1Δ1821}, α2δ1, β_{2b}), β1AR and Rad. I_Ba was measured every 10 s, by 20-ms voltage steps from a holding potential of −80 mV to +20 mV (Fig. 8A, *right panels*), using two-electrode voltage clamp (TEVC). *Left panels* of Fig. 8A show the time course (diary) of representative experiments with Ca_V1.2α_1-FL and Ca_V1.2α_{1Δ1821}. After establishing the voltage clamp, the current initially gradually increased and then often decreased to a stable level, which we considered as the basal I_Ba (denoted by the dotted line in the diaries in Fig. 8A). This baseline stabilization process took 5–15
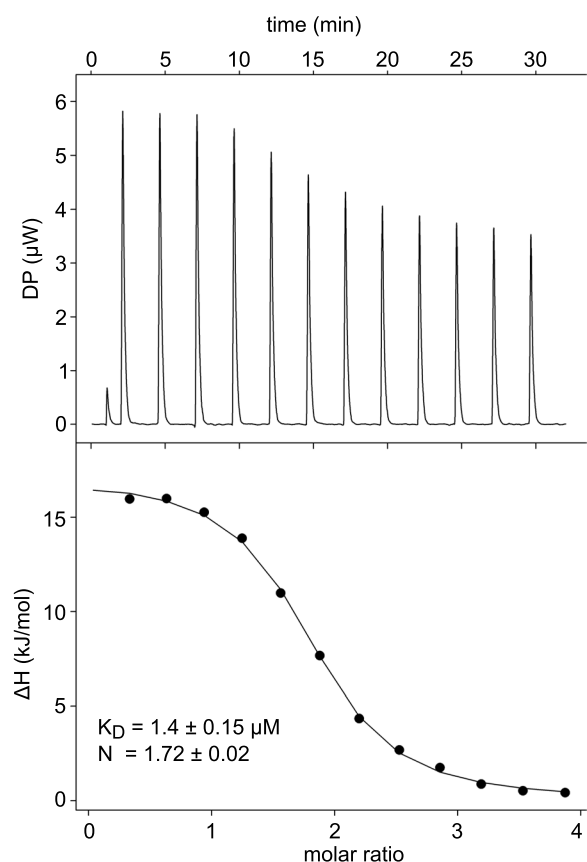
Oz *et al. BMC Biology*   (2024) 22:276

Page 9 of 22

Fig. 6 Calorimetric measurement for the titration of His-SUMO-PCRD into His-PKAC. In the top panel, data are shown as an injection profile of His-SUMO-PCRD [syringe; 400 μM] into His-PKAC (cell). The power output in DP (μW) was measured as a function of time in minutes. The heat of dilution of buffer and both proteins were subtracted and the area under the curve was integrated to generate the points that represent heat exchange in kJ/mol and plotted against the His-SUMO-PCRD to His-PKAC molar ratio for each injection, shown in the bottom panel. The solid line represents the best-fit curve for the data. Inset: thermodynamic parameters describing the fit, where *N* is the stoichiometry between PCRD and PKAC. The other thermodynamic parameters were: $\Delta G = -9.0$ cal/mol; $\Delta H = 4.1 \pm 0.77$ cal/mol; $-T\Delta S = -12.1$ cal/mol. Representative of two experiments

min. Addition of Iso (200 nM) following the stabilization of basal I_{Ba} increased the current (Figs. 8A, Additional File 1: Fig. S9A); the effect reached its maximum usually after 6–12 min (up to 17 min in rare cases). We aligned the time courses of Iso-induced $Ca_V1.2$ current increase (expressed as percent of the maximal increase in each cell) for $Ca_V1.2\alpha_1$ and $Ca_V1.2\alpha_{1\Delta1821}$. We found no statistically significant difference in the kinetics of Iso effect on FL and truncated channel (Additional File 1: Fig. S9B).

We next compared the extent of Iso-induced increase in I_{Ba} from data collected from 72 ($Ca_V1.2\alpha_1$) and 80 ($Ca_V1.2\alpha_{1\Delta1821}$) cells. On average, there was no statistically significant difference in Iso-induced increase in I_{Ba} between the FL and the truncated channel (Fig. 8B). Nevertheless, a closer examination of raw data revealed a negative correlation between the basal I_{Ba} and the Iso effect in $Ca_V1.2\alpha_{1\Delta1821}$ that was absent in full-length channels (Fig. 8C,D). To illustrate this difference in a simpler way, we divided basal I_{Ba} into arbitrarily chosen ranges, from data collected for all cells from all experiments. The effect of Iso on full-length or $Ca_V1.2\alpha_{1\Delta1821}$ channels was compared for each I_{Ba} range group using t-test. Figure 8F shows that Iso caused a significantly higher response in $Ca_V1.2\alpha_{1\Delta1821}$ compared to the FL channel when the basal current was low, but this tendency disappeared and in fact reversed when the current was high (over 700 nA) (Fig. 8E). We have re-analyzed the raw data of the previously reported series of experiments (Fig. 4 in [56]) and found the same general tendencies, with a negative correlation between basal I_{Ba} and fold-increase by Iso in the truncated, but not the FL channel (Fig. S9). Thus, the PKA modulation of FL and $\Delta1821$ $Ca_V1.2$ differs mechanistically, possibly involving the tripartite PCRD-DCRD-PKAC interactions.

Discussion

βAR regulation of $Ca_V1.2$ is achieved mainly via phosphorylation of channel-associated Rad [76] by PKAC following its separation from PKAR. Since AKAPs are not essential for this regulation in cardiomyocytes [52, 53], we hypothesized that PKA may interact directly with $Ca_V1.2\alpha_1$. Using several independent methods, we showed here that PKAC interacts directly with $Ca_V1.2\alpha_1$, and have mapped two regulatory domains on $Ca_V1.2\alpha_1$-CT, PCRD, and DCRD, that bind PKAC in the absence of PKAR. We also show that PCRD and DCRD interact with each other. The functional role of these interactions is currently unclear. We did not find evidence for a regulation of PKA catalytic activity by PCRD or DCRD (Additional File 1: Fig. S8), but found a subtle but significant difference in β1AR regulation of full-length vs. dCT-truncated (lacking the DCRD) $Ca_V1.2$ in a heterologous model system.

Our first main finding is a direct interaction between PKAC and $Ca_V1.2$, via $Ca_V1.2\alpha_1$. This is suggested by co-immunoprecipitation (co-IP) of PKAC and $Ca_V1.2\alpha_1$ in rat left ventricles and a heterologous expression model (HEK293 cells). The results from HEK293 cells show that this interaction is independent on the presence of PKAR or AKAPs, because PKAC-YFP shows co-IP with $Ca_V1.2\alpha_{1\Delta1821}$ independently of AKAP, PKAR, or dCT expression, and their interaction is not impaired by activation of PKA, which separates PKAC from PKAR (Fig. 2). In support, PKAC was found in a close association with the channel following βAR stimulation in
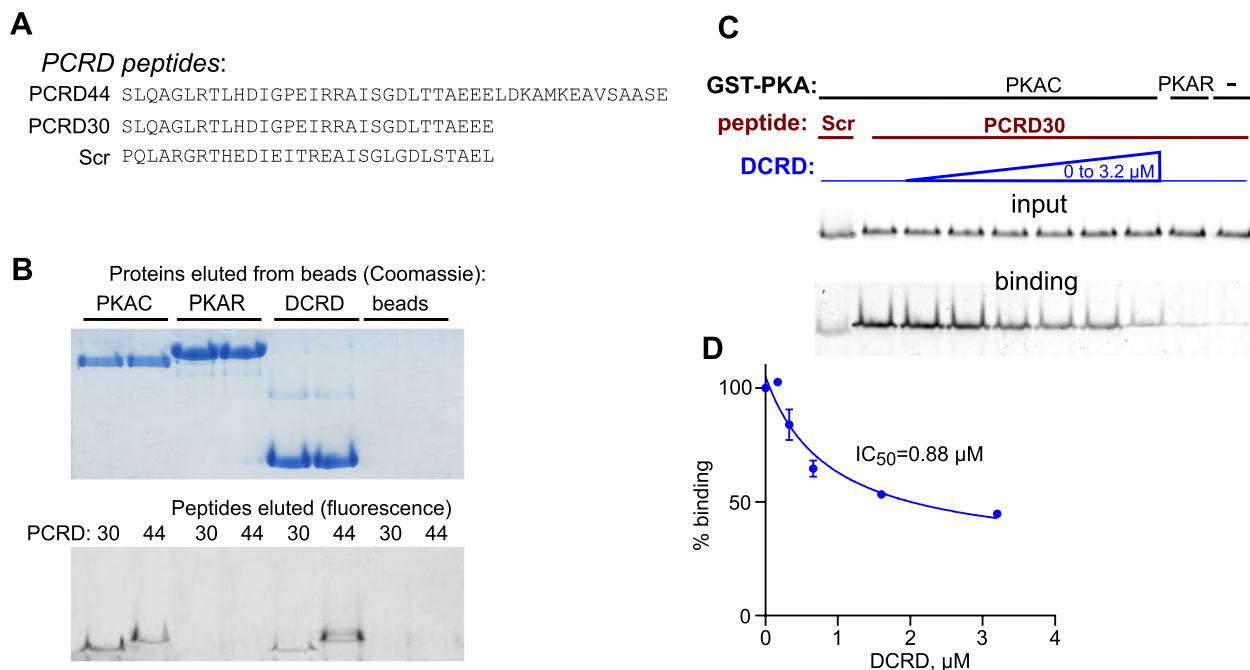
A

PCRD peptides:
PCRD44 SLQAGLRTLHDIGPEIRRAISGDLTTAEEELDKAMKEAVSAASE
PCRD30 SLQAGLRTLHDIGPEIRRAISGDLTTAEEE
    Scr PQLARGRTHEDIEITREAISGLGDLSTAEL

B

Proteins eluted from beads (Coomassie):
PKAC   PKAR   DCRD   beads

Peptides eluted (fluorescence)
PCRD: 30 44 30 44 30 44 30 44

C

GST-PKA: PKAC   PKAR −
peptide: Scr   PCRD30
DCRD: 0 to 3.2 µM
input
binding

D

$IC_{50}=0.88$ µM

Fig. 7 PKAC and DCRD, but not PKA-RIIβ, bind the PCRD peptides. **A** Fluorescein-labeled peptides used were PCRD44 and PCRD30. Scrambled (Scr) peptide was used as a negative control. **B** His-PKAC and His-DCRD, but not His-PKA-RIIb, bind the PCRD44 and PCRD30. The binding reaction was performed with 10 µg of each protein and peptide. Proteins were eluted from Ni–NTA beads and separated on a 16.5% polyacrylamide gel with Tricine buffer (1% SDS). SDS was not present in the sample buffer. Upper, Coomassie staining; lower, imaging of fluorescein-labeled PCRD peptides. **C** DCRD impedes the PKAC/PCRD interaction. Binding reaction was performed with 250 nM GST-PKAC or GST-PKA-RIIb, 2.5 µM PCRD peptides, and increasing concentrations of His-DCRD (from 0 to 3.2 µM). Pull-down was done with glutathion affinity beads. **D** Summary of 3 experiments as in **C**. Each point shows mean ± SEM. To construct the binding curve, data were fitted to a standard binding isotherm in the form [% of control = min + (max−min)/(1 + (X/IC$_{50}$))], yielding a half-inhibition concentration (IC$_{50}$) of 0.88 µM, maximal (max) binding of 105.2%, minimal (min) binding level of 25.6%

cardiomyocytes, i.e., after separation of PKAC from PKAR, by a proximity assay [55]. Further, we have unequivocally established direct, mutual binding of purified recombinant PKAC with synthetic peptides and purified recombinant segments of Ca$_V$1.2α$_1$ (PCRD, DCRD) using rigorous biochemical and biophysical methods, pull-down, and isothermal titration calorimetry (ITC) (Figs. 3, 4, 5, 6, and 7). Importantly, since in HEK293 the PKAC co-precipitates with the dCT-less Ca$_V$1.2α$_{1\Delta1821}$, the dCT (with its AKAP-binding sites) is also not essential; the PKAC interaction with Ca$_V$1.2α$_{1\Delta1821}$ probably occurs via PCRD. It must be emphasized, however, that the fact that co-IP of Ca$_V$1.2α$_1$ with PKAC in rat ventricle and in HEK293 cell takes place in the absence of PKA activation, suggests that the PKA holoenzyme can also bind Ca$_V$1.2α$_1$.

Our second major finding is the existence of a tripartite interaction, where PKAC interacts with two domains in Ca$_V$1.2α$_1$, which, in turn, also interact with each other. We have mapped the binding sites and characterized the interaction between PKAC and Ca$_V$1.2α$_1$, first using peptide array analysis for both proteins, and then corroborating the findings by pulldown and ITC, using purified recombinant parts of Ca$_V$1.2α$_1$ (PCRD$_{trunc}$ and DCRD) and synthetic PCRD peptides. The peptide array analysis identified the PCRD and DCRD domains in Ca$_V$1.2α$_1$-CT as the main sites of interaction with PKAC (Fig. 3). Following this discovery, we produced purified PCRD and DCRD and mapped their interaction sites on a PKAC peptide array. The results pointed to two PCRD-interacting domains on PKAC, one of them overlapping a DCRD-binding domain (Fig. 4). Further studies may be needed to better delineate the exact DCRD and PCRD binding sites in PKAC.

Importantly, both pull-down titration and ITC experiments (Figs. 5, 6) revealed dose-dependent and saturating binding of PCRD$_{trunc}$ and DCRD to PKAC, corroborating specific binding. ITC, which accurately estimates the thermodynamic parameters of protein interactions, determined the affinity of PKAC/PCRD$_{trunc}$ interaction to be the low-micromolar range. Although we used truncated PCRD and the exact truncation site is unknown, the pulldown experiments with the PCRD44 and PCRD30 peptides confirmed that the main binding site is located
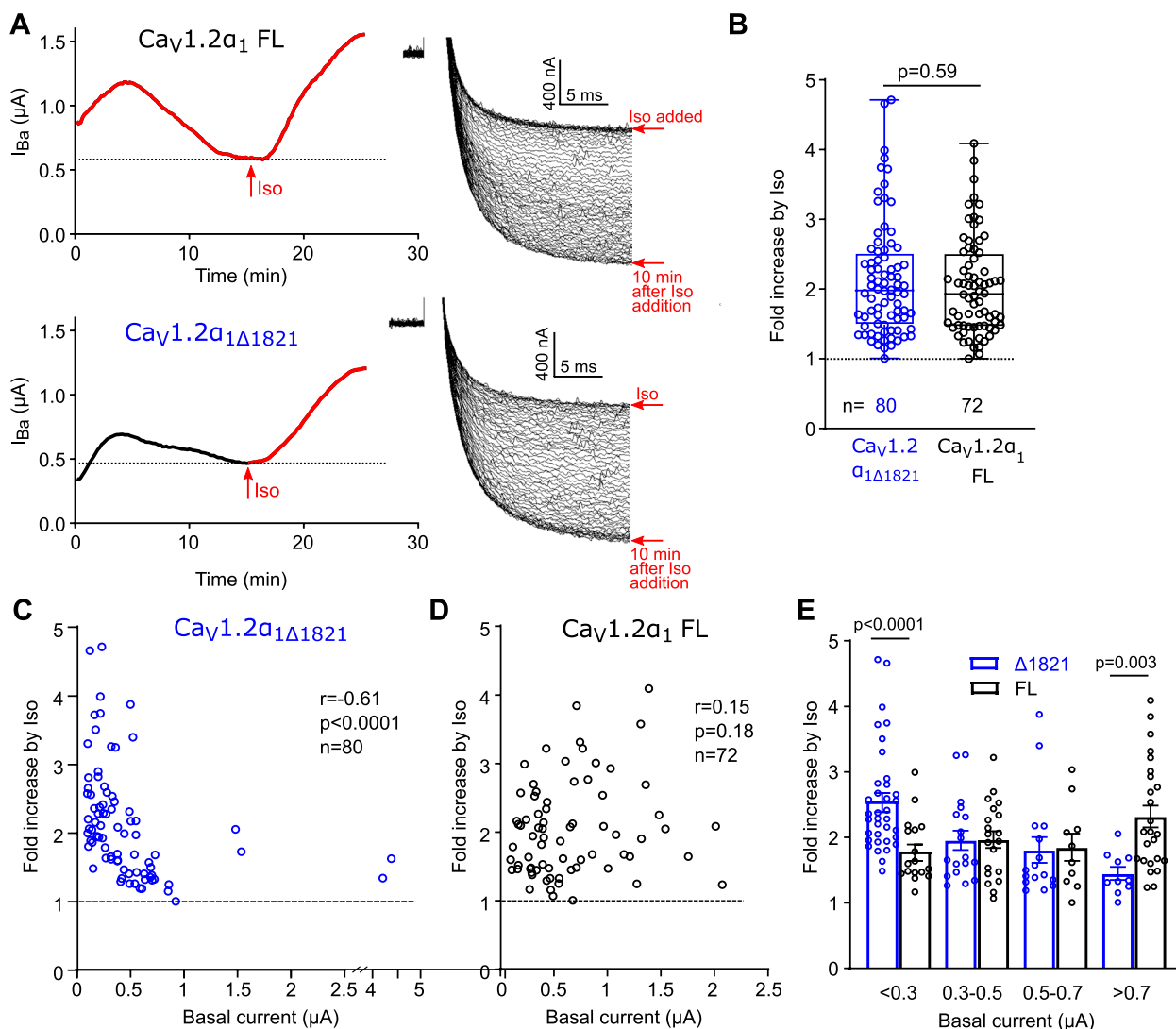
Fig. 8 Quantitative differences in β1AR regulation of full-length and truncated $Ca_V1.2$. **A** Time course (diary) of changes in I_{Ba} with time (*left panels*), and original I_{Ba} records (*right panels*). Data from representative oocytes expressing $Ca_V1.2\alpha_1$ FL $Ca_V1.2$ (*top*) and $Ca_V1.2\alpha_{1\Delta1821}$ $Ca_V1.2$ (*bottom*) are shown. Oocytes expressed $Ca_V1.2\alpha_1$ (FL or Δ1821), β_{2b}, α2δ1, Rad, and β1AR. I_{Ba} was measured by 20-ms depolarization steps from −90 to +20 mV every 10 s, starting shortly after electrode insertion (*t*=0). Iso (200 nM) was applied at the indicated time (red arrows). The right panels show consecutive current records (separated by 10-s intervals) starting at the time of application of Iso. Most of the capacity transient (an upward deflection preceding the actual inward I_{Ba}) has been erased for clarity. The recording was stopped when I_{Ba} reached a steady level, as witnessed by the last 3–4 overlapping current traces (~ 10 min after Iso addition in the examples shown here). **B** Summary of Iso-induced increase in all oocytes expressing $Ca_V1.2\alpha_{1\Delta1821}$ (*n*=80) and $Ca_V1.2\alpha_1$ FL (*n*=72). All cells from all experiments have been are included, no outlier exclusion has been performed. There was no significant difference between the two groups (two-tailed Mann–Whitney test, *U*=2735). Here and in **D**, **E** the dotted line indicates fold increase of 1 (no effect of Iso). **C**, **D** Correlation between basal I_{Ba} and fold increase by Iso in individual cells. Parameters of Spearman correlation analysis for the two distributions are shown in insets. **E** Comparison of differences in Iso-induced increase in I_{Ba} of $Ca_V1.2\alpha_{1\Delta1821}$ and $Ca_V1.2\alpha_1$ FL for basal I_{Ba} of small, intermediate and high amplitude. Results from all cells from all experiments have been subdivided into 4 subgroups according to their I_{Ba} amplitudes, and in each subgroup, we summarized the extent of Iso-induced increase in the current (shown on *Y*-axis). Mean±SEM is shown. In each subgroup of amplitudes, the difference between $Ca_V1.2\alpha_1$ FL and $Ca_V1.2\alpha_{1\Delta1821}$ was analyzed by Mann–Whitney unpaired test except for currents > 0.7 μA where the data distributions passed the Shapiro–Wilk normality test, and an unpaired *t*-test was performed

within $PCRD_{trunc}$. These peptides contain the GPEIR-RAISG motif, where the penultimate serine is S^{1700}, known to be phosphorylated by PKA [2]. (In contrast,

there are no known or potential PKA phosphorylation sites in the DCRD). A transient interaction between the PCRD and PKAC could be expected, as PCRD contains

Oz *et al. BMC Biology*   (2024) 22:276

Page 12 of 22

the PKAC-target motif RRxxS [92]. The homology of this segment in PCRD to high-affinity PKA-binding pseudo-substrate sites of PKAR and PKI (Additional File 1: Fig. S5F) further increase our confidence that this is a major PKA-binding segment in PCRD. Interestingly, a recent study did not detect significant binding between PKAC and a short 18-mer peptide RTLHDIGPEIRRAISGDL from PCRD, using ITC [93]. This implies that additional residues (present in our PCRD$_{trunc}$), either upstream or downstream from that sequence, are involved in PKAC binding. Furthermore, there may be an additional binding segment even beyond PCRD$_{trunc}$ indicated by the peptide array (Fig. 3), so that the actual affinity of this interaction may be higher than 1 μM. ITC also revealed an apparent stoichiometry of 1.7 that is in line with the presence of two potential PCRD-binding sites in PKAC (Fig. 4). Further study is needed to determine the exact stoichiometry of PKAC/PCRD interaction.

The binding of PKAC to both PCRD and DCRD is remarkable, since the interaction between the two domains is envisaged as part of the mechanism by which Ca$_V$1.2α$_1$-dCT inhibits channel's gating. A direct interaction between PCRD and DCRD was predicted, using a computational model, to exist via salt bridges between specific residues (including R^{1696} and R^{1697} of PCRD) on both domains [24]. Dissociation of PCRD from DCRD, induced by phosphorylation of S^{1700}, was proposed to mediate the Ca$_V$1.2 regulation by PKA [2]. However, our demonstration (ref. [56] and Fig. 8) of full βAR/PKA regulation of dCT-truncated Ca$_V$1.2, which is Rad dependent, rules out this mechanism. Nevertheless, our results (Fig. 7B) provide solid experimental evidence for a direct PCRD-DCRD interaction. In support, Lyu et al. [94] demonstrated interaction between two large segments of the Ca$_V$1.2α$_1$-CT, one including the EF, pre-IQ, IQ, and PCRD domains in the proximal Ca$_V$1.2α$_1$-CT and the other including DCRD and CCD (downstream of DCRD) in the Ca$_V$1.2α$_1$-dCT. This interaction was inhibited by CaM in a Ca^{2+}-dependent manner. In addition, the authors reported an interaction between segments of proximal and distal Ca$_V$1.2α$_1$-CT that contained neither PCRD nor DCRD [94]. In Ca$_V$1.3 channels, three domains were suggested to interact and to compete with CaM: PCRD, DCRD, and IQ$_V$ (preIQ$_3$-IQ domain), modulating both activation and inactivation of the channel [95]. Overall, it appears that PCRD/DCRD-dependent and additional interactions between the proximal and distal CT in Ca$_V$1.2α$_1$ and Ca$_V$1.3α$_1$ profoundly regulate the channel's function and possibly its regulation by Ca/calmodulin and PKA.

It was intriguing to find that the same 30-a.a. motif within PCRD (the PCRD30 peptide) interacts both with PKAC and DCRD (Fig. 7), and that DCRD and PCRD share overlapping binding sites on PKAC (Fig. 4). This suggested a compound interaction module in which all three binding partners might compete for a common binding site. The triple interaction experiment showed a concentration-dependent reduction in PKAC/PCRD30 binding by DCRD (Fig. 7). Nevertheless, the displacement of the PCRD30 peptide by DCRD was incomplete, suggesting that a significant fraction of PCRD30 may remain bound to PKAC, simultaneously with DCRD. This is plausible, in view of the presence of a second PCRD-interacting segment in PKAC, which does not overlap the DCRD-binding site (Fig. 4). In the inverse competition protocol, the PCRD30 peptide was unable to reduce DCRD/PKAC binding. While this may result from a lower affinity of this peptide to the common PCRD/DCRD site on PKAC, it may also reflect more complex mechanisms involving mutual interactions between the three parties. Future in-depth experiments will be needed in order to further understand the qualitative and quantitative aspects of this tripartite interaction.

Taken together, our data on tripartite PKAC-PCRD-DCRD interactions indicate both partial competition and possible simultaneous interactions of the three partners. Pairwise interactions may carry specific functions of their own (such as inhibition of channel's activity by DCRD-PCRD interaction in full-length channels). We further propose that the tripartite interactions discovered here may serve as a platform for assisting the colocalization of PKA with the channel, within βAR-Ca$_V$1.2 multimolecular signaling complexes. AKAP may or may not be present but it is not essential. After activation of the PKA holoenzyme by cAMP, PKAC remains associated with the truncated Ca$_V$1.2α$_1$, presumably via PCRD (Fig. 2) and PCRD does not impair PKAC's catalytic activity. Hence, we speculate that PCRD may serve as a "hub" for PKA-Ca$_V$1.2 interactions, and the dissociated PKAC monomer may remain a part of Ca$_V$1.2 multimeric complex. Figure 9 illustrates this hypothesis.

There are several lines of evidence that support the idea of a PKA-Ca$_V$1.2 dynamic complex based on PKAC—Ca$_V$1.2α$_1$ interactions. The incomplete displacement of PCRD30 by DCRD is one. Another one is the affinity of interaction. The low-μM PKAC-PCRD$_{trunc}$ binding affinity is typical for a dynamic biological regulation [96]. Notably, the affinity of PKAC for its phosphorylation substrates tends to be lower, enabling the fast turnover necessary for efficient catalysis [97]. Thus, one to two orders of magnitude lower affinity was found in three best-phosphorylated peptide substrates related to Ca$_V$1.2 regulation, one from Ca$_V$1.2α$_1$ (containing the S1928 phosphorylation site) and two from Rad [93]. In that study, the 18-mer PCRD peptide (RTLHDIGPEIRRAISGDL) was a poor
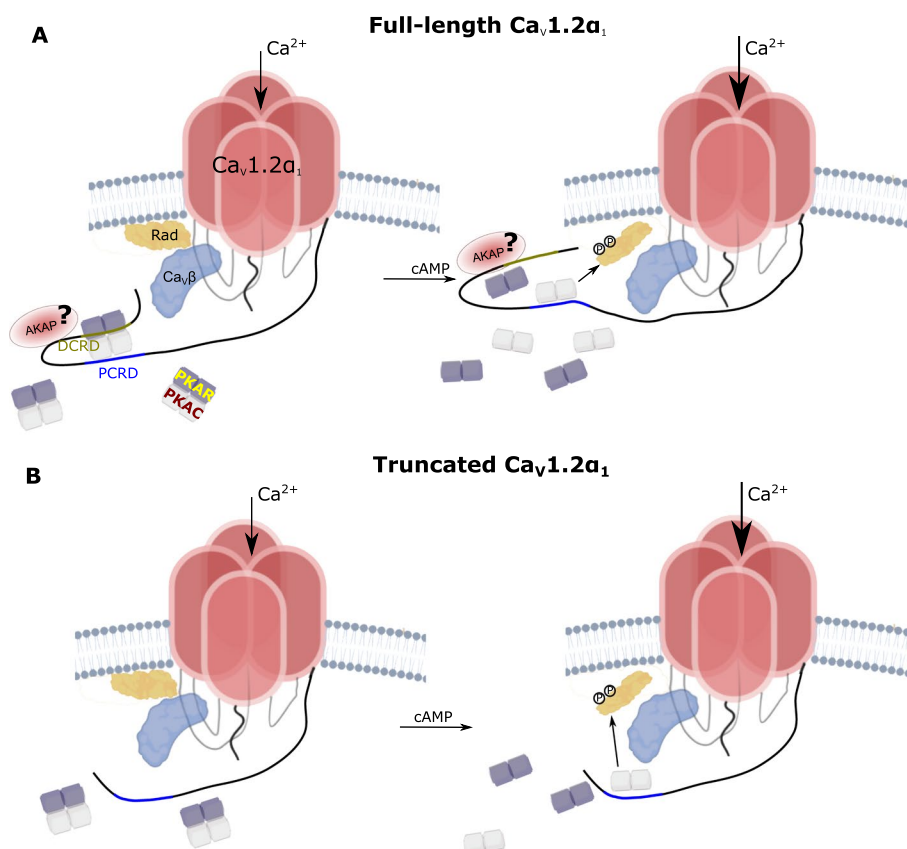
Fig. 9 A tentative scheme of the involvement of PCRD and DCRD in PKA regulation of $Ca_V1.2$ with full-length (**A**) and truncated (**B**) $Ca_V1.2\alpha_1$. The $\alpha2\delta$ subunit is not shown, for simplicity. PKAC can directly interact with $Ca_V1.2\alpha_1$ both in the PKA holoenzyme and after separation from PKAR. The main sites of $Ca_V1.2\alpha_1$ interaction with PKAC are DCRD and PCRD. In the full-length channel, the tripartite interactions (DCRD-PKAC, PCRD-PKAC, and DCRD-PCRD) are proposed to contribute to the maintenance of a multimolecular signaling complex of the PKA holoenzyme with the CT of $Ca_V1.2\alpha_1$, ensuring high local concentration of PKA in channel's vicinity. In cardiac cells, the complex may contain additional components such as β2AR that can bind the dCT of $Ca_V1.2\alpha_1$ [15] and, potentially, AKAP. In the oocyte model system, AKAP is most probably not present and is not essential for β-AR regulation [56]. The interaction between DCRD-PCRD is not explicitly illustrated but may play a modulatory role. Upon activation of β-AR, increase in cAMP levels and the dissociation of PKAC and PKAR, PKAC phosphorylates Rad which dislocates from the plasma membrane and relieves channel's inhibition, increasing Ca^{2+} influx [77]. In the truncated channel lacking the DCRD, the complex is less well organized and the effect of cAMP is mediated mainly by the available PKA from the cytosole, which may be in short supply when the surface density of Ca^{2+} channels is high. Therefore, a negative correlation between basal I_{Ca} and the effect of Iso was observed for the truncated channel, whereas in the full-length channel the effect of Iso remained constant in a wide range of channel densities. Both in full-length and truncated $Ca_V1.2$, PKAC may remain attached to the PCRD while catalyzing the phosphorylation of Rad

substrate for phosphorylation by PKAC. Therefore, the functional role of the PCRD-PKAC interaction may indeed not be phosphorylation of S1700. Although PKAC will not be obligatorily "anchored" to the PCRD site, it may be enriched in that nanodomain due to kinetic scaffolding [98]. This potential mechanism facilitates localized signaling by restraining PKAC diffusion [99]. The third indication comes from the electrophysiological data as discussed below.

In mammalian heterologous models, both full-length [55] and truncated [65] $Ca_V1.2$ are upregulated by elevated cAMP. However, the *Xenopus* oocyte is the only heterologous expression system in which the entire

cascade can be reconstituted when $Ca_V1.2$, βAR, and Rad are coexpressed [56]. Therefore, we addressed the role of dCT by studying the regulation of the channel by β1AR activation in the oocytes expressing the channel, β1AR and Rad (note that coexpression of Rad was dispensable for co-immunoprecipitation of $Ca_V1.2$ and PKAC, as in Fig. 2, but essential for reconstituting the β-adrenergic pathway, i.e. for functional assays). On average, $Ca_V1.2$-FL and the truncated $Ca_V1.2\alpha_{1\Delta1821}$ were similarly upregulated by β1AR activation by the agonist, isoproterenol (Iso), in terms of the average extent of Iso regulation and its kinetics. However, an in-depth analysis of the regulation according to basal

Oz et al. BMC Biology (2024) 22:276

Page 14 of 22

current before Iso application (which may correspond to the number of functional channels) revealed a difference between the two forms of the channel. We found a negative correlation between the basal current and the extent of Iso-induced regulation in $Ca_V1.2\alpha_{1\Delta1821}$, but not in $Ca_V1.2\alpha_1$-FL (Fig. 8). This analysis has several limitations, such as possible differences in the ratio of expressed channel subunits to Rad (which may affect the extent of βAR regulation), yet the reproducibility of these results in two separate series of experiments (Fig. 8 and Additional File 1: Fig. S9C-E) supports the validity of our observations. These findings highlight the differences in the physiological regulation of the two forms of the channel by PKA and indicate specific functions of the dCT in βAR regulation. We note that our present functional study, focused on the role of $Ca_V1.2\alpha_1$-dCT, gives only an initial indication for an involvement of dCT (and thus, potentially, the discovered tripartite interactions) in the adrenergic regulation of $Ca_V1.2$. More extensive future studies will be needed to better understand the role of the discovered $Ca_V1.2$-PKAC interactions.

Our observations are in line with a previously reported negative correlation between the $Ca_V1.2$ basal current and the magnitude of βAR regulation in cardiomyocytes [100, 101]. This correlation was observed both in untreated cardiomyocytes and in cells overexpressing $Ca_V\beta$ subunits. It was proposed [100] that there may be a limiting factor, such as a finite number of permissive sites on the membrane, where PKA-mediated upregulation of $Ca_V1.2$ can occur. When the amount of channel protein exceeds the amount of the limiting factor, a further increase in the channel's surface density results in a subpopulation of $Ca_V1.2$ irresponsive to PKA. Among such factors, we can think about available PKA or Rad; indeed, not all channels are constitutively associated with Rad [67, 75]. We propose that the tripartite interaction between PCRD/DCRD/PKAC may also stabilize the PKA – $Ca_V1.2$ association in the full-length $Ca_V1.2\alpha_1$, ensuring sufficient PKA for full βAR regulation even at high membrane densities of $Ca_V1.2$. The role of the secondary $Ca_V\beta$-binding domain in the dCT, located very close to DCRD (Fig. 1), is unknown and will need to be investigated. It is possible that it further contributes to the formation of the macromolecular complex by physically or "kinetically" scaffolding both $Ca_V\beta$ and the associated Rad in the proximity of $Ca_V1.2\alpha_1$-CT and PKAC. In the truncated form ($Ca_V1.2\alpha_{1\Delta1821}$) of the channel, such multimolecular interactions may be absent or less tight, thus either Rad or PKAC may not be sufficiently recruited to channel's vicinity, becoming limiting factors.

Conclusions

In summary, we show that PKAC directly binds to two regulatory domains on the CT of $Ca_V1.2\alpha_1$ (PCRD and DCRD) independently of PKAR or the need for AKAPs. These two domains also interact with each other. We propose that dCT modulates the βAR regulation of $Ca_V1.2$, possibly by supporting the scaffolding of a macromolecular complex of $Ca_V1.2$ with PKAC and Rad, which may contribute to an efficient βAR regulation of the channel.

Methods

Animal use and ethical approval

Experiments were approved by Tel Aviv University Institutional Animal Care and Use Committee (IACUC permit # 01–20–083). Female frogs were kept in tanks filled with dechlorinated water that was exchanged 3 times a week, at 20 ± 2 °C on 10 h light/14 h dark cycle. Frogs were anaesthetized in 0.17–0.2% tricaine methanesulfonate (MS-222), and portions of ovary were removed through an incision on the abdomen. The incision was sutured, and the animal was held in a separate tank until it had fully recovered from the anesthesia, and afterwards was returned to a separate tank for post-operational animals. The animals did not show any signs of post-operational distress and were allowed to recover for at least 3 months until the next surgery. Following the final collection of oocytes (or the 4th surgery as defined by the IACUC rules), anaesthetized frogs were sacrificed by decapitation and double pithing.

DNA constructs and RNA

For transient expression in HEK293T cells, the following constructs were used: mouse PKAC-YFP in pcDNA3 (mouse PKAC, GenBank: NM_008854, fused to eYFP, GenBank: GQ221700.1) PKA- RIIβ-HA (GenBank: NM 001020020.1; the HA tag was fused in frame at the end of the C-terminus). For protein purification from *E. coli*, the following constructs were used: His-tagged Cα-subunit of PKA (His-PKAC, GenBank:NM 008854.5), glutathion-S-transferase (GST)-fused PKA-RIIβ (GST-PKAR; GenBank: NM 001030020) [85], GST-fused Cα-subunit of mouse PKA, GST-PKAC (GenBank: NM008854.4) (kind gift from S.S. Taylor). In addition, we have produced DNA constructs for protein production in *E. coli* in pET-Duet vector, encoding the following proteins: (1) His_8-SUMO-PCRD, with a 3 a.a. segment MGS followed by an 8-His (His_8) tag fused to SUMO (a.a. 1–81 of human Chain B of small ubiquitin-related modifier 2; PDB: 2IO3_B) further fused via a ENLYFQG liker (a TEV protease cleavage site) to PCRD (a.a. G1671-T1751 of rabbit $Ca_V1.2\alpha_1$). 2) His_8-DCRD-Myc, with an

MGS-His$_8$ tag fused via a TEV digestion site to DCRD (a.a. R2058-S2120 of rabbit Ca$_V$1.2α_1) followed by a Myc tag, EQKLISEEDL.

RNA for *Xenopus* oocyte injections was transcribed in vitro using previously described protocols and DNA constructs [56, 85]: human Rad (NP_001122322), cardiac long-N terminus isoform of rabbit Ca$_V$1.2α_1 (GenBank: X15539), rabbit Ca$_V\beta_{2b}$ (GenBank: X64297.1), rabbit $\alpha2\delta1$ (GenBank: M21948), mouse $\beta1$ adrenergic receptor (NP_031445.2). For oocyte expression, the coding sequences of these DNAs were inserted into pGEM-SB or pGEM-HJ vectors containing the 5′ and 3′ untranslated regions of *Xenopus* β-globin [102].

Ca$_V$1.2 was expressed in *Xenopus* oocytes in full subunit composition Ca$_V$1.2$\alpha_1 + \alpha2\delta + \beta_{2b}$, by injection of equal amounts, by weight, of RNAs of each subunit. To obtain similar ranges of amplitudes of I$_{Ba}$ for Ca$_V$1.2α_1-FL and Ca$_V$1.2$\alpha_{1\Delta1821}$, and to ensure optimal Rad-dependent regulation by Iso, we tested a range of RNA doses for the channel subunits and Rad. For experiments shown here we chose the following combination of RNA doses, per oocyte: Ca$_V$1.2α_1: 2 ng for Ca$_V$1.2α_1-FL and 1 ng for Ca$_V$1.2$\alpha_{1\Delta1821}$; 0.5 ng Rad RNA for Ca$_V$1.2α_1-FL and 1 ng Rad for Ca$_V$1.2$\alpha_{1\Delta1821}$. RNA of $\beta1$AR was 10–20 pg/oocyte.

Electrophysiology in *Xenopus* oocytes
Oocytes were defolliculated by collagenase treatment [103], injected with the desired combinations of RNAs, and incubated for 3 days at 20–22 °C in NDE solution (in mM: 96 NaCl, 2 KCl, 1 MgCl$_2$, 1 CaCl$_2$, 5 Hepes, 2.5 pyruvic acid, and 0.1 gentamycin sulfate). Recordings started 3 days after RNA injection and conducted over the next 2 days. Comparison of basal currents between test groups was performed on recordings from the same day. Results of "before-after Iso" analysis of each oocyte (Iso) were pooled from all the recordings performed over 2–3 days. Oocytes of the various experimental groups were tested intermittently over the entire duration of the experiment to normalize variability, as protein levels increase over time. Oocytes were placed in a recoding chamber (solution volume ~ 100 μl) perfused at a steady rate, that did not change throughout the experiment, with 40 mM Ba^{2+} solution (in mM: 40 Ba(OH)$_2$, 50 NaOH, 2 KOH, and 5 Hepes, titrated to pH 7.5 with methanesulfonic acid). The chamber was connected via 3 M KCl bridges and silver chloride-coated electrodes to the ground inputs of the virtual ground module of the Geneclamp 500 amplifier (Molecular Devices, Sunnyvale, CA, USA). Currents were recorded using two-electrode voltage clamp in virtual ground mode [104], digitized with Digidata 1440A, and acquired and analyzed with the pCLAMP software (Molecular Devices, Sunnyvale, CA, USA). I$_{Ba}$

was elicited by depolarizing pulses from a holding potential of − 80 mV to + 20 mV applied at 10-s intervals. The voltage step to + 20 mV was preceded by a hyperpolarizing prepulse to − 90 mV (100 ms), to estimate the leak conductance. Net I$_{Ba}$ was calculated by subtracting the calculated leak currents during the analysis session. Iso (Sigma-Aldrich, I5627) was diluted in water, aliquoted, and stored in 100 mM stock solution at − 20 °C. Perfusion of isoproterenol (200 nM) began after attaining a stable peak current for about 2 min (see Fig. 8).

Generation and culture of the inducible mouse Ca$_V$1.2a HEK293 cell line
To generate the inducible mouse Ca$_V$1.2a 293 cells, stop codon was introduced after Val1821 in mouse Ca$_V$1.2a (isoform 7, NM_001255999.2) and its cDNA subcloned into the pcDNA5/FRT vector. After transfection, the Flp-In TRex HEK293 (Flp-In-293, Invitrogen) cells were selected in the presence of Hygromycin B (100 μg/ml) and single clones were grown and analyzed by Western blot before and after tetracycline-induced mouse Ca$_V$1.2a cDNA expression (Additional File 1: Fig. S1A). Cells were induced for 18 h with 1 μg /ml tetracycline (Invitrogen). The cells were cultured in Dulbecco's modified Eagle's medium (DMEM 41965–039, Gibco, Thermo Fisher Scientific, Waltham, USA), supplemented with 10% fetal bovine serum (FBS, Gibco), and 200 mM L-Glutamine, 100 μg/ml Hygromycin B, and 100 U / ml Penicillin with 100 μg/ ml Streptomycin at 37 °C and 5% CO$_2$.

HEK293 cells were maintained in Dulbecco's modified Eagle's medium (DMEM) supplemented with 10% fetal bovine serum (FBS), 100 U/ml penicillin, 10 mg/ml streptomycin, and 2 mM L-Glutamine (Biological Industries) at 37 °C with 5% CO$_2$. Transient transfection with the calcium-phosphate was 48 h before the cells were collected.

Immunoprecipitation from HEK293 cells
For activation of adenylyl cyclase, cells were incubated for 10 min with DMSO (1:1000) or with 25 μM forskolin (Alomone, stock 10 mM in DMSO). Cells were scrapped in PBS + 0.5 mM phenylmethylsulfonyl fluoride (PMSF) at 4 °C and cell pellets were stored at − 80 °C. Cell pellets were solubilized in *lysis buffer*: 1% Triton × 100, 20 mM Tris pH 7.5, 20 mM EDTA, 10 mM EGTA + protease inhibitors (cOmplete, Roche), 25 mM β-glycerolphosphate, 2 mM orthovanadate, and 0.5 mM PMSF, for 30 min on ice then cleared by centrifugation at max speed. Supernatants were transferred for protein quantification (Lowry assay) and immunoprecipitation (IP). For IP, 900 μg total protein were diluted in 300 μl lysis buffer, and 25 μg total protein were taken as input. Samples were incubated with ~ 1.5 μg IP antibody at 4 °C in a rotating device, overnight. For Ca$_V$1.2α_1, we used 2 μl IP

antibody (ACC-003, Alomone, 0.8 mg/ml) and for $Na_V1.1$ we added 2.5 µl (ASC-001, Alomone, 0.6 mg/ml). Protein A-Sepharose beads (GE17-0780–01, 50 µl) were taken for each tested sample from the slurry and incubated overnight with 0.5% BSA in PBS, then washed with PBS and lysis buffer. Then an equal amount of washed beads was divided per sample and incubated at 4 °C for 90 min in a rotating device. Beads were washed on a rotating device, at RT, three times with 1 ml *washing buffer*: 1% Triton×100, 20 mM Tris pH 7.5, 150 mM NaCl, and 0.5 mM PMSF, and a final wash with 20 mM Tris pH 7.5 and 0.5 mM PMSF. When indicated, 1 mM cAMP (Sigma-Aldrich, stock 20 mM in DDW) were added to the washing buffer. Proteins were eluted by incubation with sample buffer for 5 min at 65 °C and centrifuged, and the clear supernatant was taken for acrylamide-gel loading and Western blot analysis.

Co-immunoprecipitation of Ca$_V$1.2 and PKAC from heart

The left ventricles from male Sprague–Dawley rats were isolated and stored at − 80 °C. Tissue samples were homogenized in a lysis buffer containing 1% Triton×100, 20 mM Tris pH 7.5, 20 mM EDTA, 10 mM EGTA, freshly supplemented with protease inhibitors cocktail (A32955, Thermo Fisher Scientific), 25 mM β-glycerol-phosphate, 2 mM sodium orthovanadate, and 0.5 mM PMSF using a rotor–stator homogenizer and then incubated for 30 min on a rotating device (4 °C). Lysates were centrifuged at 3000 rpm for 15 min at 4 °C. The supernatants were collected, and the protein concentration was measured using the Coomassie Plus Bradford protein assay (Thermo Fisher Scientific, 1856210). For immunoprecipitation, 900 µg of total protein was incubated with 4.8 µg of Anti-CaV1.2 (ACC-003, Alomone Labs) or an equal amount of normal rabbit IgG (2729, Cell Signaling) in 300 µl lysis buffer overnight at 4 °C on a rotating device. Sepharose A beads were washed (3x) with PBS and coated with 0.5% BSA (4 °C, overnight, on a rotating device). The following day, excess BSA was removed by washing with PBS (3x), and a final wash with a lysis buffer without inhibitors. Slurry beads (50 µl, 1:1 with lysis buffer) were added to each sample and incubated for 90 min at 4 °C. The beads with immunoprecipitated complexes were washed (3x) with a washing buffer containing 1% Triton×100, 20 mM Tris pH 7.5, and 150 mM NaCl and fleshly supplemented 0.5 mM PMSF, and a final wash with 20 mM Tris pH 7.5 and fleshly supplemented 0.5 mM PMSF. Proteins were eluted by incubation with 2×Laemmli buffer supplemented with 2-ME for 5 min at 65 °C, centrifuged, and loaded on a PAGE gel (4–20% or 7.5% pre-cast gels, Bio-Rad). Seventy-five micrograms of protein from the input samples was loaded onto the same gel. Samples were electrophoresed on PAGE gels

and transferred onto PVDF membranes (Towbin buffer, 36 V, 16 h). The membranes were blocked with 3% BSA for 1 h at room temperature and incubated with primary antibodies (1:400 for anti-CaV1.2, ACC-003, Alomone Labs; 1:1000 for anti-PKA cat α BD Biosciences, 610980) at 4 °C overnight. The following day, the membranes were washed with TBS-T (3x), incubated with the corresponding HRP-coupled secondary antibodies for 1 h at room temperature, and washed with TBS-T (3x). Proteins were detected using Immobilon® Western chemiluminescent HRP substrate (Millipore, WBKLS0500) and imaged on an Odyssey Imager (LI-COR Biosciences).

Electrophysiology in HEK293 cells

Currents were recorded using whole-cell patch-clamp configuration, and sampled at 10 kHz. Signals were amplified using an Axopatch 200B patch-clamp amplifier, digitized with Digidata 1440A and analyzed using pCLAMP 10 software (Axon Instruments). External solution contained (mM): 150 Tris, 10 glucose, 1 $MgCl_2$, and 10 $BaCl_2$ (adjusted to pH 7.4 with methanesulphonic acid). The intracellular solution contained (mM) 135 $CsCl_2$, 10 EGTA, 1 $MgCl_2$, 4 MgATP, 10 Hepes (pH 7.3, adjusted with CsOH).

Production and purification of recombinant proteins

Recombinant proteins were all expressed in *E. coli* (BL21-DE3 and derivatives and produced using standard methods, essentially as described [85, 105]. Freshly transformed colonies were inoculated into 2xYT media, grown at 37° C, induced with IPTG (0.25–1 mM) at OD=0.4–0.6. Growth after induction was at 16–24 °C overnight, or, for GST-PKAC, 6.5 h at 24 °C. Bacterial cells were harvested by centrifugation, frozen, and stored at − 20 or − 80° C for later use.

For His-tag proteins, defrosted bacterial paste was resuspended in lysis buffer: potassium phosphate, pH 8 (50 mM), 0.1 M NaCl, β-mercaptoethanol 5 mM or PBS pH 7.8 with β-mercaptoethanol (2 mM). DNase, lysozyme, and PMSF and protease inhibitor cocktail (solution or tablets) were added to facilitate lysis and inhibit proteolysis. Cells were lysed either by microfluidizer or sonication. The lysate was then centrifuged at high RCF for 30–60 min and soluble material was loaded on a Ni–NTA metal-chelate column. The resin was then spun down at 3000 rpm and the supernatant removed. The column was washed with buffer A (lysis buffer including 10 mM imidazole) and HisTag protein was eluted with buffer B (lysis buffer including either 250 or 150 mM imidazole). Fractions were pooled, concentrated, and loaded onto a SEC column (Superdex 75) equilibrated with either potassium phosphate pH 7.5 (20

Oz *et al. BMC Biology*   (2024) 22:276

Page 17 of 22

mM), KCl (20 mM), DTT (2 mM), or PBS pH 7.8 with β-mercaptoethanol (2 mM).

GST-fused proteins were purified as described [85]. Lysis was as above. Soluble lysate was then loaded on a glutathione-agarose column and eluted with glutathione. The eluate was then pooled, concentrated, and further purified using size-exclusion chromatography on Superdex-75 in the following buffer, in mM: 20 KH2PO4, 20 KCl, 2 DTT, pH 7.5. After purification, protein fractions were concentrated, frozen by flash freezing in liquid nitrogen and stored at -80 °C for later use.

Reversed-phase (RP) HPLC
Reversed-phase (RP) HPLC of uncleaved and cleaved forms of His-SUMO PCRD was performed on an JASCO PU-1580i HPLC system equipped with a UV detector (PU-1575) and flow cell (JASCO Inc. Japan). The mobile phase included water with 0.1% trifluoroacetic acid (TFA) in solvent A and 100% acetonitrile (ACN) with 0.1% TFA in solvent B. Vydac C4 semi-preparative RP column with 5 μm particle size and column dimensions 240 mm×10 mm were used for the HPLC runs. The columns were operated at room temperature with a flow rate of 0.5 mL/ min. The column eluate was analyzed by UV detector and collected manually and further run on 12% SDS-PAGE gels for analyses. Each HPLC run lasted for approximately 80 min with a 0–100% gradient of Water:ACN was achieved in the end of 80 min.

Nano LC ESI–MS/MS mass spectrometry and raw data analysis
Lyophilized protein was reconstituted in deionized water at a concentration of 12.5 μg/μl. Fifteen micrograms was digested in solution with SMART Digest™ Trypsin magnetic beads (Thermo Fisher) at a total volume of 200 μl at 70 °C for 2 h. ten micrograms μg of reconstituted protein was digested in 0.05 N HCl with 1 μg pepsin (Promega) without prior reduction/alkylation at a volume of 200 μl 50 °C for 3 h. Nano-LC–ESI–MS/MS was performed as described previously [106] using a LTQ Orbitrap Velos Pro coupled to Ultimate 3000 RSLC nano system equipped with an Ultimate3000 RS autosampler (Thermo Fisher Scientific, Dreieich, Germany). Peptides were separated on a reversed phase column (nano viper Acclaim PepMap capillary column, C18; 2 μm; 75 μm×50 cm, ThermoFisher) at a flow rate of 200 nl/min increasing organic acetonitrile phase for 60 min as described before. We used a combination of alternate the collision induced dissociation (CID) fragmentation and high energy collision dissociation (HCD) top3 method, where full scan MS spectra (m/z 300–1700) were recorded in the orbitrap analyzer with resolution of $r=60,000$. The 3 most intense peptide ions with charge states > 2 were

sequentially isolated and fragmented in the HCD collision cell with normalized collision energy of 30%. The resulting fragments were detected in the Orbitrap system with resolution $r=7500$. For the collision induced dissociation (CID) MS/MS top3 method, full scan MS spectra (m/z 300–1700) were acquired in the Orbitrap analyzer using a target value of 10^6. The 3 most intense peptide ions with charge states > 2 were fragmented in the high-pressure linear ion trap by low-energy CID with normalized collision energy of 35%.

Tryptic and peptic peptides were analyzed by Mascot/ Proteome Discoverer 1.4 (Thermo Scientific). Raw files were searched against a SwissProt database containing 16.992 *mus musculus* entries and the manually added sequence of tagged PCRD$_{trunc}$. MS^2 spectra were matched with a mass tolerance of 7 ppm for precursor masses and 0.5 Da for peptide fragment ions. Database search was done with "no specific" enzyme digestion. Dynamic peptide modifications as oxidation at methionine, deamidation at asparagine, and glutamine and acetylation of lysine and the N-terminus and carbamidomethylation at cysteine were allowed. The mass spectrometry proteomics data have been deposited to the ProteomeXchange Consortium via the PRIDE [107] partner repository with the dataset identifier PXD057841 and https://doi.org/10.6019/PXD057841.

Pull-down of purified proteins and synthetic peptides
Procedures were essentially as described [85]. Interaction of His-fused proteins with other purified proteins (e.g., GST-PKAC) or synthetic peptides was studied by pulldown using Ni–NTA affinity resin (HisPur, ThermoScientific # 88,221). GST-fused proteins were pulled down on glutathione-Sepharose beads (Amersham Biosciences). The binding buffer contained 150 mM KCl, 5 mM MgCl$_2$, 50 mM Tris–HCl (pH=7.5), 0.025% TWEEN-20 or 0.5% CHAPS, and 1 mM EDTA. The binding reaction (300 μl total volume) was initiated by mixing the interacting proteins or peptides. After 60 min incubation on a shaker at room temperature (or 2 h at 4 °C when pull-down was done with GST-fused proteins), 5 μl of the reaction mixture was removed to later visualize the loaded proteins ("input"). At this stage, for pull-down on Ni–NTA beads, 3 μl of 1 M imidazole and 30 μl of Ni–NTA agarose beads (Thermo Scientific, MA, USA) were added to the mixture and incubated for 30 min at 4–8 °C, then washed 3 times with 500 μl of the incubation buffer containing 10 mM imidazole. Elution was done by 10 min incubation at room temperature with 30 μl of the incubation buffer containing 250 mM imidazole. For pull-down on glutathion beads, glutathione-Sepharose beads (30 μl) were added to the incubation mixture (to immobilize the GS-fused

Oz *et al. BMC Biology*   (2024) 22:276

Page 18 of 22

protein) for 60 min at 4 °C, and washed three times with 500 µl of the binding buffer. Then the buffer was removed, 20 µl of $\times 2$ sample buffer (2% SDS, 10% β-mercaptoethanol, 8% glycerol, 50 mM Tris, pH 6.5) was added to the beads, followed by incubation for 5 min at 95 °C to elute the bound protein from the beads, addition of 20 µl water, and centrifugation for 2 min at 1000 rpm in a tabletop centrifuge. The protein eluates from Ni–NTA or glutathion beads and the "input" were separately subjected to SDS–polyacrylamide (12%) gel electrophoresis (SDS-PAGE). Running buffer contained 25 mM Tris, 192 mM glycine, 1% SDS, pH 8.3. The synthetic fluorescein-labeled peptides were pulled down in the same way, but dissolved in SDS-free sample buffer, and instead of standard SDS-PAGE we used 0.75 mm thick, 16.5% Tricine gels. The running buffers contained cathode buffer 10X (upper buffer): 0.1 M Tris, 0.1 M Tricine, 0.1% SDS, pH 8.25; anode buffer: 0.2 M Tris, pH 8.9. The gels were imaged immediately after the end of electrophoresis with Fusion FX7 (Witec AG, Sursee, Switzerland) (excitation 500–550 nm, emission filter F595Y3) and subsequently stained with Coomassie Brilliant Blue G-250 (Bio-Rad #1610406) 0.1%, 8% ammonium sulfate, 1% orthophosphoric acid, and 20% ethanol.

Western blot and antibodies

Nitrocellulose membranes were blotted with protein samples and incubated for 1 h in 5% skin milk in PBS, supplemented with 0.5% Tween 20. Incubation with the primary antibody was overnight at 4 °C, and for secondary antibody, 1 h at room temperature. Membranes were incubated with chemiluminescent HRP substrate solution (SuperSignal West Pico, Thermo Scientific) and exposed to a film. The following antibodies were used as indicated: GFP, G1544 Sigma Aldrich (rabbit); $Ca_V1.2$ ($Ca_V1.2\alpha_1$), ACC003, Alomone; PKAC SC-903 (PKAα), Santa Cruz (rabbit); $Na_V1.1$, ASC-001 Alomone; HA antibody, Santa Cruz SC7392, mouse; His6 Peroxidase, Roche 11965085001; Cavβ (in-house for β3 and β2; PMID: 21357697). Secondary antibodies: goat anti rabbit (Jackson, 111–035–1440); mouse anti rabbit light chain (Jackson, 211–032–171). Densitometry of bands was using ImageJ (NIH). In experiments of Fig. 2, for Western blots, we used 2 µl of anti-$Ca_V1.2$ (ACC-003; 0.8 mg/ml) and 2.5 µl of anti-$Na_V1.1$ (ASC-001; 0.6 mg/ml); see Table S1. Normalized level of co-IP was the co-IP band intensity divided by the band intensity of IP, e.g., when PKAC-YFP was immunoprecipitated, co-IP normalized level was calculated as: $Ca_V1.2\alpha_1 = (Ca_V1.2\alpha_1/PKAC\text{-}YFP)$; (PKAR-HA)/(PKAC-YFP). Normalized co-IP level for a treatment was divided by normalized co-IP of control (e.g., DMSO).

Peptide spot array of $Ca_V1.2\alpha_1$ cytosolic segments and of PKAC

Peptide array of N-terminal and C-terminal parts of rabbit $Ca_V1.2\alpha_1$ (X15539) and an N-terminal segment of human $Ca_V1.2\alpha_1$ (XP_006719080.1) was spot-synthesized as 25-mer peptides overlapping sequences, shifted by 5 a.a. along the sequence, using AutoSpot Robot ASS 222 (Intavis Bioanalytical Instruments, Cologne, Germany), as described previously [108]. Peptides were generated by automatic SPOT synthesis and blotted on a Whatman membrane. The interaction with spot-synthesized peptides was investigated by an overlay assay. Following blocking (1 h, RT) with 5% BSA in 20 mM Tris and 150 mM NaCl with 0.1% Tween-20 (TBST), 0.1–0.02 µM purified His-PKAC were incubated with the immobilized peptide-dots, overnight at 4 °C. PKAC was detected by PKAC antibody (sc-903) and HRP-coupled secondary antibody incubated with 5% BSA/TBST, and the membrane was exposed to a sensitive film or imaged with Fusion FX7, as for immunoblotting. Mouse PKACα (NM_008854) was spot-synthesized as above for $Ca_V1.2\alpha_1$ and incubated with 0.1 µM recombinant His-DCRD-Myc or His-SUMO-PCRD at 4 °C overnight in 50 mM Tris pH 7.4, 5 mM $MgCl_2$. Successful binding was analyzed using anti-His tag antibody (PCRD, Invitrogen #MA1-135) or anti-Myc Tag (DCRD, Cell Signaling Technologies #2276).

Isothermal titration calorimetry

Isothermal titration calorimetry was measured on a MicroCal PEAQ-ITC (Malvern) to examine the interaction between HisTag-SUMO PCRD and HisTag-PKAC. HisTag-SUMO-PCRD and HisTag-PKA were both prepared in the same buffer (PBS pH 7.8 supplemented with 2 mM β-ME) and were degassed before each experiment. Titrations were performed by injecting of His-SUMO-PCRD [400 µM] (syringe) into of His-PKAC [20 µM] (cell) at 25 °C. Each experiment consisted of 13 injections and the time interval between each injection was 150 s. The cell volume was ~ 200 µl while the syringe contained ~ 75 µl prior to each experiment. Three control experiments were performed under the same conditions and were subtracted from the experimental dataset: (i) HisTag-SUMO-PCRD [400 µM] in syringe and buffer in cell; (ii) buffer in syringe and HisTag-PKAC [20 µM] in cell; (iii) buffer versus buffer. Data obtained were fit to a one site binding model with the manufacturer's software.

Oz *et al. BMC Biology*   (2024) 22:276

Page 19 of 22

Cook assay

Human PKA-Cα was overexpressed in E. coli BL21(DE3) cells after induction with 0.4 mM isopropyl-β-D-1-thiogalactopyranoside (IPTG) for 16 h at room temperature using the expression vector pRSETb-hPKACα and then purified by affinity chromatography using an IP20-resin as described earlier [109]. Kinase activity of human PKAC in the presence of the two channel fragments was determined in a coupled spectrophotometric assay as described previously [110]. The assay buffer contained 100 mM MOPS (pH 7), 10 mM $MgCl_2$, 1 mM phosphoenolpyruvate, 1 mM ATP, 2.5 mM β-Mercaptoethanol, 15 U/mL lactate dehydrogenase (Roche Diagnostics GmbH, Mannheim, Germany), 8.4 U/mL pyruvate kinase (Roche Diagnostics GmbH, Mannheim, Germany), 0.1 mg/mL BSA, and 200 mM NADH. For the measurement, 1 μM or 10 μM of His-DCRD-Myc or His-SUMO-PCRD was added to 100 μL assay mix. Thirty nanomolar of human PKAC was added, and the reaction started by addition of 260 μM S-Kemptide (LRRASLG; GeneCust) at room temperature. NADH depletion was measured using a spectrophotometer (Specord 205, Analytic Jena) at a wavelength of 340 nm for 30 s. The slope of each measurement was calculated in the WinAspect software (Informer Technologies) and the values exported to Graphpad Prism 9.0 for statistical analysis.

ADP-Glo assay

The ADP-Glo™ Assay (Promega, Germany) is a luminescence-based kinase assay in which the amount of produced ADP is proportional to the luminescence signal. Here, 20 nM bovine PKAC was incubated with Kemptide as substrate in PKA kinase buffer (40 mM Tris–HCl, pH 7.4, 20 mM $MgCl_2$, 0.1 mg/mL BSA, 50 μM DTT). Ten micromolar of His-DCRD-Myc or His-SUMO-PCRD was added to the reaction mix. To inhibit kinase activity, 30 μM of H89 was added. Samples were diluted in PKA kinase buffer and reactions set up in a 384-well plate. Kinase reaction was done for 5 min at room temperature. The reaction was stopped by addition of 5 μL ADP Glo reagent and the plate incubated for 40 min at room temperature. Ten microliters of kinase detection reagent was added and the plate incubated for 30 min at room temperature. The luminescence was recorded using Tecan plate reader (Tecan, Mannedorf, Switzerland) with an integration time of 0.5 s. Antibodies used were as follows: mouse anti-Hsp90 (Enzo Life Science, #SPA-830); mouse anti-GFP Tag (Thermo Fisher Scientific, #MA5-15,256); rabbit anti-pPKA substrate (Cell Signaling Technology, #9621).

Statistical analysis

Statistical analysis was performed in GraphPad Prism (GraphPad, La Jolla, Ca, USA). Data were tested for normality of distribution using the Shapiro–Wilk test. In case of normal distribution, pairwise comparison was done by *t*-test and multiple comparisons by one-way ANOVA with post hoc Bonferroni or Sidak-Holm correction. If the data did not pass normal distribution test, they were analyzed using Mann–Whitney (pairwise) and Kruskal–Wallis non-parametric ANOVA tests.

Abbreviations

a.a.	Amino acid
AKAP	A-kinase anchoring protein
βAR	β-Adrenergic receptor
CaM	Calmodulin
CBS	C-terminal β-binding site
CT	C-terminus
DCRD	Distal C-terminal regulatory domain
dCT	Distal C-terminus
FL	Full-length
PCRD	Proximal C-terminal regulatory domain
PKA	Protein Kinase A
PKAC	Protein Kinase A catalytic subunit
PKAR	Protein Kinase A regulatory subunit

Supplementary Information

The online version contains supplementary material available at https://doi.org/10.1186/s12915-024-02076-9.

Additional File 1. Supporting information.PDF. This file contains: Figure S1, related to Fig. 2. Generation of HEK293 cells stably transfected with CaV1.2α1 truncated at 1821 and Ba currents in these cells. Figure S2, related to Fig. 2. PKAC co-immunoprecipitates with CaV1.2α1 from rat heart. Figure S3, related to Fig. 3. The full peptide array membrane of CaV1.2α1 N- and C-terminal 25 a.a. peptides. Figure S4, related to Fig. 4. His-DCRD-Myc: purification from E. coli. Figure S5, related to Fig. 4. His-SUMO-PCRD: purification and analysis. Figure S6, related to Fig. 5. SUMO does not bind PKAC. Figure S7, related to Fig. 7. The PCRD30 peptide does not reduce the interaction between His-DCRD and GST-PKAC. Figure S8. PCRD and DCRD do not alter the catalytic activity of PKAC. 'Figure S9, related to Fig. 8. β1AR regulation of full-length and truncated CaV1.2: kinetics of Iso effect and additional analysis of published results. Table S1. Antibodies used in this study.

Additional File 2. "Original gels.rar". The file contains original images of gels or Western blots that were trimmed in main or supplementary figures. The images are in TIFF or PNG forms and, in some cases, summaries of the separate gels with explanations or captions, in the form of PDF or PPT files. Included: a separate file "Original gels for Fig. S2.png" and directories: "Original gels for Fig. 2A,B"; "Original gels for Fig. 7C"; "Original gels for Fig. 8A".

Authors' contributions

ND, SO, SW, MK, JAH, VF, EK, and FWH conceived the study and supervised experiments; SO, TS, MK, TP, SS, VT, DRT, GS, LV, CFT, TKR, DB, JAH, AS, and KZ planned, performed, and analyzed experiments; DRT, BW, OCH, and MS created and provided new materials (DNAs and proteins); SW, ND, JAH, EK, and SO wrote the paper. All authors participated in the editing of the manuscript. All authors read and approved the final manuscript.

Oz *et al. BMC Biology*   (2024) 22:276

Page 20 of 22

Data availability

All data generated or analyzed during this study are included in this published article, its supplementary information files, and publicly available repositories. The full MS data are available via ProteomeXchange with identifier PXD057841. Materials (new DNA constructs) will be available upon request.

Declarations

Ethics approval and consent to participate

Experiments were approved by Tel Aviv University Institutional Animal Care and Use Committee (IACUC permit # 01–20-083).

Consent for publication

Not applicable.

Competing interests

The authors declare that they have no competing interests.

Author details

[1]School of Medicine, Faculty of Medical and Health Sciences, Tel Aviv University, 6997601 Tel Aviv, Israel. [2]Department of Neuroscience, Faculty of Medicine, The Ruth and Bruce Rappaport, Haifa 3109601, Israel. [3]School of Neurobiology, Biochemistry and Biophysics, Faculty of Life Sciences, Tel Aviv University, Tel Aviv 6997601, Israel. [4]Max-Delbrück-Center for Molecular Medicine in the Helmholtz Association (MDC), Berlin, Germany. [5]Heart Center, Sheba Medical Center, Ramat Gan 5262000, Israel. [6]Experimentelle Und Klinische Pharmakologie & Toxikologie, Universität Des Saarlandes, Homburg 66421, Germany. [7]Department of Biochemistry, University of Kassel, Heinrich-Plett-Str. 40, Kassel 34132, Germany. [8]DZHK (German Centre for Cardiovascular Research), Partner Site Berlin, Germany. [9]National Forensic Science University, Radhanagar, Agartala, Tripura 799001, India.

References

1. Bers DM. Calcium cycling and signaling in cardiac myocytes. Annu Rev Physiol. 2008;70:23–49.
2. Catterall WA. Regulation of cardiac calcium channels in the fight-or-flight response. Curr Mol Pharmacol. 2015;8(1):12–21.
3. Taylor SS, Knighton DR, Zheng J, Ten Eyck LF, Sowadski JM. cAMP-dependent protein kinase and the protein kinase family. Faraday Discuss. 1992;93:143–52.
4. Taylor SS, Zhang P, Steichen JM, Keshwani MM, Kornev AP. PKA: lessons learned after twenty years. Biochim Biophys Acta. 2013;1834(7):1271–8.
5. Best JM, Kamp TJ. Different subcellular populations of L-type Ca^{2+} channels exhibit unique regulation and functional roles in cardiomyocytes. J Mol Cell Cardiol. 2012;52(2):376–87.
6. Nikolaev VO, Moshkov A, Lyon AR, Miragoli M, Novak P, Paur H, et al. Beta2-adrenergic receptor redistribution in heart failure changes cAMP compartmentation. Science. 2010;327(5973):1653–7.
7. Pallien T, Klussmann E. New aspects in cardiac L-type Ca^{2+} channel regulation. Biochem Soc Trans. 2020;48(1):39–49.
8. Dikolayev V, Tuganbekov T, Nikolaev VO. Visualizing cyclic adenosine monophosphate in cardiac microdomains involved in ion homeostasis. Front Physiol. 2019;10:1406.
9. Maurya S, Mills RW, Kahnert K, Chiang DY, Bertoli G, Lundegaard PR, et al. Outlining cardiac ion channel protein interactors and their signature in the human electrocardiogram. Nat Cardiovasc Res. 2023;2(7):673–92.
10. Venetucci L, Denegri M, Napolitano C, Priori SG. Inherited calcium channelopathies in the pathophysiology of arrhythmias. Nat Rev Cardiol. 2012;9(10):561–75.
11. Sanchez-Alonso JL, Fedele L, Copier JS, Lucarelli C, Mansfield C, Judina A, et al. Functional LTCC-β_2AR complex needs caveolin-3 and is disrupted in heart failure. Circ Res. 2023.
12. Xiao RP, Cheng H, Zhou YY, Kuschel M, Lakatta EG. Recent advances in cardiac beta(2)-adrenergic signal transduction. Circ Res. 1999;85(11):1092–100.
13. Xiao RP, Zhu W, Zheng M, Chakir K, Bond R, Lakatta EG, et al. Subtype-specific β-adrenoceptor signaling pathways in the heart and their potential clinical implications. Trends Pharmacol Sci. 2004;25(7):358–65.
14. Balijepalli RC, Foell JD, Hall DD, Hell JW, Kamp TJ. Localization of cardiac L-type Ca^{2+} channels to a caveolar macromolecular signaling complex is required for β_2-adrenergic regulation. Proc Natl Acad Sci U S A. 2006;103(19):7500–5.
15. Davare MA, Avdonin V, Hall DD, Peden EM, Burette A, Weinberg RJ, et al. A b2 adrenergic receptor signaling complex assembled with the Ca^{2+} channel Ca_V1.2. Science. 2001;293(5527):98–101.
16. Tsien RW, Giles W, Greengard P. Cyclic AMP mediates the effects of adrenaline on cardiac purkinje fibres. Nat New Biol. 1972;240(101):181–3.
17. Weiss S, Oz S, Benmocha A, Dascal N. Regulation of cardiac L-type Ca^{2+} channel Ca_V1.2 via the β-adrenergic-cAMP-protein kinase A pathway: old dogmas, advances, and new uncertainties. Circ Res. 2013;113(5):617–31.
18. Roybal D, Hennessey JA, Marx SO. The quest to identify the mechanism underlying adrenergic regulation of cardiac Ca^{2+} channels. Channels (Austin). 2020;14(1):123–31.
19. Man KNM, Navedo MF, Horne MC, Hell JW. β2 adrenergic receptor complexes with the L-type Ca^{2+} channel Ca_V1.2 and AMPA-type glutamate receptors: paradigms for pharmacological targeting of protein interactions. Annu Rev Pharmacol Toxicol. 2020;60:155–74.
20. Catterall WA, Perez-Reyes E, Snutch TP, Striessnig J. International Union of Pharmacology. XLVIII. Nomenclature and structure-function relationships of voltage-gated calcium channels. Pharmacol Rev. 2005;57(4):411–25.
21. Zamponi GW, Striessnig J, Koschak A, Dolphin AC. The physiology, pathology, and pharmacology of voltage-gated calcium channels and their future therapeutic potential. Pharmacol Rev. 2015;67(4):821–70.
22. Dolphin AC. Voltage-gated calcium channels and their auxiliary subunits: physiology and pathophysiology and pharmacology. J Physiol. 2016;594(19):5369–90.
23. Hell JW, Westenbroek RE, Warner C, Ahlijanian MK, Prystay W, Gilbert MM, et al. Identification and differential subcellular localization of the neuronal class C and class D L-type calcium channel α 1 subunits. J Cell Biol. 1993;123(4):949–62.
24. Hulme JT, Yarov-Yarovoy V, Lin TW, Scheuer T, Catterall WA. Autoinhibitory control of the CaV1.2 channel by its proteolytically processed distal C-terminal domain. J Physiol. 2006;576(Pt 1):87–102.
25. Katchman A, Yang L, Zakharov SI, Kushner J, Abrams J, Chen BX, et al. Proteolytic cleavage and PKA phosphorylation of α1C subunit are not required for adrenergic regulation of Ca_V1.2 in the heart. Proc Natl Acad Sci U S A. 2017;114(34):9194–9.
26. Bannister JP, Leo MD, Narayanan D, Jangsangthong W, Nair A, Evanson KW, et al. The voltage-dependent L-type Ca^{2+} (Ca_V1.2) channel C-terminus fragment is a bi-modal vasodilator. J Physiol. 2013;591(12):2987–98.
27. Dai S, Hall DD, Hell JW. Supramolecular assemblies and localized regulation of voltage-gated ion channels. Physiol Rev. 2009;89(2):411–52.
28. Satin J, Schroder EA, Crump SM. L-type calcium channel auto-regulation of transcription. Cell Calcium. 2011;49(5):306–13.
29. Buonarati OR, Henderson PB, Murphy GG, Horne MC, Hell JW. Proteolytic processing of the L-type Ca^{2+} channel $α_1$1.2 subunit in neurons. F1000Res. 2017;6:1166.
30. Hell JW, Westenbroek RE, Breeze LJ, Wang KK, Chavkin C, Catterall WA. N-methyl-D-aspartate receptor-induced proteolytic conversion of postsynaptic class C L-type calcium channels in hippocampal neurons. Proc Natl Acad Sci U S A. 1996;93(8):3362–7.

Oz et al. BMC Biology   (2024) 22:276

Page 21 of 22

31. Wei X, Neely A, Lacerda AE, Olcese R, Stefani E, Perez Reyes E, et al. Modification of Ca^{2+} channel activity by deletions at the carboxyl terminus of the cardiac a$_1$ subunit. J Biol Chem. 1994;269(3):1635–40.

32. Gao T, Cuadra AE, Ma H, Bunemann M, Gerhardstein BL, Cheng T, et al. C-terminal fragments of the a$_{1C}$ (Ca$_V$1.2) subunit associate with and regulate L-type calcium channels containing C-terminally truncated a$_{1C}$ subunits. J Biol Chem. 2001;276:21089–97.

33. Fu Y, Westenbroek RE, Scheuer T, Catterall WA. Basal and β-adrenergic regulation of the cardiac calcium channel Ca$_V$1.2 requires phosphorylation of serine 1700. Proc Natl Acad Sci U S A. 2014;111(46):16598–603.

34. Fuller MD, Emrick MA, Sadilek M, Scheuer T, Catterall WA. Molecular mechanism of calcium channel regulation in the fight-or-flight response. Sci Signal. 2010;3(141):ra70.

35. Davare MA, Horne MC, Hell JW. Protein phosphatase PP2A is associated with class C L-type calcium channels (Ca$_V$1.2) and antagonizes channel phosphorylation by cAMP-dependent protein kinase. J Biol Chem. 2000;275(50):39710–7.

36. Hall DD, Davare MA, Shi M, Allen ML, Weisenhaus M, McKnight GS, et al. Critical role of cAMP-dependent protein kinase anchoring to the L-type calcium channel Ca$_V$1.2 via A-kinase anchor protein 150 in neurons. Biochemistry. 2007;46(6):1635–46.

37. Lin C, Guo X, Lange S, Liu J, Ouyang K, Yin X, et al. Cypher/ZASP is a novel A-kinase anchoring protein. J Biol Chem. 2013;288(41):29403–13.

38. Marshall MR, Clark JP 3rd, Westenbroek R, Yu FH, Scheuer T, Catterall WA. Functional roles of a C-terminal signaling complex of Ca$_V$1 channels and A-kinase anchoring protein 15 in brain neurons. J Biol Chem. 2011;286(14):12627–39.

39. Ganesan AN, Maack C, Johns DC, Sidor A, O'Rourke B. β-adrenergic stimulation of L-type Ca^{2+} channels in cardiac myocytes requires the distal carboxyl terminus of α1C but not serine 1928. Circ Res. 2006;98(2):e11–8.

40. Gomez-Ospina N, Tsuruta F, Barreto-Chang O, Hu L, Dolmetsch R. The C terminus of the L-type voltage-gated calcium channel Ca(V)1.2 encodes a transcription factor. Cell. 2006;127(3):591–606.

41. Schroder E, Byse M, Satin J. L-type calcium channel C terminus autoregulates transcription. Circ Res. 2009;104(12):1373–81.

42. Murakami AM, Nagatomo K, Miyoshi I, Itagaki S, Niwa Y, Murakami M. A novel binding site between the voltage-dependent calcium channel CaV1.2 subunit and CaVβ2 subunit discovered using a new analysis method for protein-protein interactions. Sci Rep. 2023;13(1):13986.

43. Subramanian H, Nikolaev VO. A-Kinase anchoring proteins in cardiac myocytes and their roles in regulating calcium cycling. Cells. 2023;12(3):436.

44. Dell'Acqua ML, Smith KE, Gorski JA, Horne EA, Gibson ES, Gomez LL. Regulation of neuronal PKA signaling through AKAP targeting dynamics. Eur J Cell Biol. 2006;85(7):627–33.

45. Skroblin P, Grossmann S, Schäfer G, Rosenthal W, Klussmann E. Mechanisms of protein kinase A anchoring. Int Rev Cell Mol Biol. 2010;283:235–330.

46. Scott JD, Pawson T. Cell signaling in space and time: Where proteins come together and when they're apart. Science. 2009;326(5957):1220–4.

47. Perino A, Ghigo A, Scott JD, Hirsch E. Anchoring proteins as regulators of signaling pathways. Circ Res. 2012;111(4):482–92.

48. Langeberg LK, Scott JD. Signalling scaffolds and local organization of cellular behaviour. Nature Revi Mol Cell Biol. 2015;16(4):232–44.

49. Murphy JG, Sanderson JL, Gorski JA, Scott JD, Catterall WA, Sather WA, et al. AKAP-anchored PKA maintains neuronal L-type calcium channel activity and NFAT transcriptional signaling. Cell Rep. 2014;7(5):1577–88.

50. Hulme JT, Lin TW, Westenbroek RE, Scheuer T, Catterall WA. Beta-adrenergic regulation requires direct anchoring of PKA to cardiac Ca$_V$1.2 channels via a leucine zipper interaction with A kinase-anchoring protein 15. Proc Natl Acad Sci U S A. 2003;100(22):13093–8.

51. Gao T, Yatani A, Dell'Acqua ML, Sako H, Green SA, Dascal N, et al. cAMP-dependent regulation of cardiac L-type Ca^{2+} channels requires membrane targeting of PKA and phosphorylation of channel subunits. Neuron. 1997;19(1):185–96.

52. Nichols CB, Rossow CF, Navedo MF, Westenbroek RE, Catterall WA, Santana LF, et al. Sympathetic stimulation of adult cardiomyocytes requires association of AKAP5 with a subpopulation of L-type calcium channels. Circ Res. 2010;107(6):747–56.

53. Jones BW, Brunet S, Gilbert ML, Nichols CB, Su T, Westenbroek RE, et al. Cardiomyocytes from AKAP7 knockout mice respond normally to adrenergic stimulation. Proc Natl Acad Sci U S A. 2012;109(42):17099–104.

54. Yu H, Yuan C, Westenbroek RE, Catterall WA. The AKAP Cypher/Zasp contributes to β-adrenergic/PKA stimulation of cardiac Ca$_V$1.2 calcium channels. J Gen Physiol. 2018;150(6):883–9.

55. Liu G, Papa A, Katchman AN, Zakharov SI, Roybal D, Hennessey JA, et al. Mechanism of adrenergic Ca$_V$1.2 stimulation revealed by proximity proteomics. Nature. 2020;577(7792):695–700.

56. Katz M, Subramaniam S, Chomsky-Hecht O, Tsemakhovich V, Flockerzi V, Klussmann E, et al. Reconstitution of β-adrenergic regulation of Ca$_V$1.2: Rad-dependent and Rad-independent protein kinase A mechanisms. Proc Natl Acad Sci USA. 2021;118(21):e2100021118.

57. Patriarchi T, Buonarati OR, Hell JW. Postsynaptic localization and regulation of AMPA receptors and Ca$_V$1.2 by β2 adrenergic receptor/PKA and Ca^{2+}/CaMKII signaling. EMBO J. 2018;37(20):e99771.

58. Patriarchi T, Qian H, Di Biase V, Malik ZA, Chowdhury D, Price JL, et al. Phosphorylation of Ca$_V$1.2 on S1928 uncouples the L-type Ca^{2+} channel from the β2 adrenergic receptor. EMBO J. 2016;35(12):1330–45.

59. Qian H, Patriarchi T, Price JL, Matt L, Lee B, Nieves-Cintron M, et al. Phosphorylation of Ser 1928 mediates the enhanced activity of the L-type Ca^{2+} channel Ca$_V$1.2 by the β2-adrenergic receptor in neurons. Sci Signal. 2017;10(463):eaaf9659.

60. Nystoriak MA, Nieves-Cintron M, Patriarchi T, Buonarati OR, Prada MP, Morotti S, et al. Ser^{1928} phosphorylation by PKA stimulates the L-type Ca^{2+} channel Ca$_V$1.2 and vasoconstriction during acute hyperglycemia and diabetes. Sci Signal. 2017;10(463):eaaf9647.

61. Dixon RE, Navedo MF, Binder MD, Santana LF. Mechanisms and physiological implications of cooperative gating of clustered ion channels. Physiol Rev. 2022;102(3):1159–210.

62. Hofmann F, Flockerzi V, Kahl S, Wegener JW. L-type Ca$_V$1.2 calcium channels: from in vitro findings to in vivo function. Physiol Rev. 2014;94(1):303–26.

63. Lemke T, Welling A, Christel CJ, Blaich A, Bernhard D, Lenhardt P, et al. Unchanged beta-adrenergic stimulation of cardiac L-type calcium channels in Ca v 1.2 phosphorylation site S1928A mutant mice. J Biol Chem. 2008;283(50):34738–44.

64. Poomvanicha M, Matthes J, Domes K, Patrucco E, Angermeier E, Laugwitz KL, et al. β-adrenergic regulation of the heart expressing the Ser1700A/Thr1704A mutated Ca$_V$1.2 channel. J Mol Cell Cardiol. 2017;111:10–6.

65. Hovey L, Gamal El-Din TM, Catterall WA. Convergent regulation of Ca$_V$1.2 channels by direct phosphorylation and by the small GTPase RAD in the cardiac fight-or-flight response. Proc Natl Acad Sci U S A. 2022;119(42):e2208533119.

66. Hovey L, Guo X, Chen Y, Liu Q, Catterall WA. Impairment of β-adrenergic regulation and exacerbation of pressure-induced heart failure in mice with mutations in phosphoregulatory sites in the cardiac Ca$_V$1.2 calcium channel. Front Physiol. 2023;14:1049611.

67. Papa A, Kushner JS, Hennessey JA, Katchman AN, Zakharov SI, Chen BX, et al. Adrenergic Ca$_V$1.2 activation via Rad phosphorylation converges at α$_{1C}$ I-II Loop. Circ Res. 2021;128(1):76–88.

68. Manning JR, Yin G, Kaminski CN, Magyar J, Feng HZ, Penn J, et al. Rad GTPase deletion increases L-type calcium channel current leading to increased cardiac contraction. J Am Heart Assoc. 2013;2(6): e000459.

69. Ahern BM, Levitan BM, Veeranki S, Shah M, Ali N, Sebastian A, et al. Myocardial-restricted ablation of the GTPase RAD results in a pro-adaptive heart response in mice. J Biol Chem. 2019;294(28):10913–27.

70. Béguin P, Nagashima K, Gonoi T, Shibasaki T, Takahashi K, Kashima Y, et al. Regulation of Ca2+ channel expression at the cell surface by the small G-protein kir/Gem. Nature. 2001;411(6838):701–6.

71. Finlin BS, Crump SM, Satin J, Andres DA. Regulation of voltage-gated calcium channel activity by the Rem and Rad GTPases. Proc Natl Acad Sci USA. 2003;100(24):14469–74.

72. Wang G, Zhu X, Xie W, Han P, Li K, Sun Z, et al. Rad as a novel regulator of excitation-contraction coupling and beta-adrenergic signaling in heart. Circ Res. 2010;106(2):317–27.

73. Sasson Y, Navon-Perry L, Huppert D, Hirsch JA. RGK family G-domain:GTP analog complex structures and nucleotide-binding properties. J Mol Biol. 2011;413(2):372–89.

Oz et al. BMC Biology   (2024) 22:276

Page 22 of 22

74. Yang T, Puckerin A, Colecraft HM. Distinct RGK GTPases differentially use α1- and auxiliary β-binding-dependent mechanisms to inhibit CaV1.2/CaV2.2 channels. PLoS One. 2012;7(5):e37079.

75. Papa A, Zakharov SI, Katchman AN, Kushner JS, Chen BX, Yang L, et al. Rad regulation of Ca$_V$1.2 channels controls cardiac fight-or-flight response. Nat Cardiovasc Res. 2022;1(11):1022–38.

76. Papa A, Kushner J, Marx SO. Adrenergic regulation of calcium channels in the heart. Annu Rev Physiol. 2022;84:285–306.

77. Papa A, Del Rivero Morfin PJ, Chen BX, Yang L, Katchman AN, Zakharov SI, et al. A membrane-associated phosphoswitch in Rad controls adrenergic regulation of cardiac calcium channels. J Clin Invest. 2024;134(5):e176943.

78. Weissgerber P, Held B, Bloch W, Kaestner L, Chien KR, Fleischmann BK, et al. Reduced cardiac L-type Ca2+ current in Ca(V)beta2-/- embryos impairs cardiac development and contraction with secondary defects in vascular maturation. Circ Res. 2006;99(7):749–57.

79. Berggren PO, Yang SN, Murakami M, Efanov AM, Uhles S, Köhler M, et al. Removal of Ca^{2+} channel β3 subunit enhances Ca^{2+} oscillation frequency and insulin exocytosis. Cell. 2004;119(2):273–84.

80. Becker A, Wardas B, Salah H, Amini M, Fecher-Trost C, Sen Q, et al. Cavβ3 regulates Ca^{2+} signaling and insulin expression in pancreatic β-cells in a cell-autonomous manner. Diabetes. 2021;70(11):2532–44.

81. Link S, Meissner M, Held B, Beck A, Weissgerber P, Freichel M, et al. Diversity and developmental expression of L-type calcium channel β2 proteins and their influence on calcium current in murine heart. J Biol Chem. 2009;284(44):30129–37.

82. Belkacemi A, Hui X, Wardas B, Laschke MW, Wissenbach U, Menger MD, et al. IP3 receptor-dependent cytoplasmic Ca^{2+} signals are tightly controlled by Ca$_V$β3. Cell Rep. 2018;22(5):1339–49.

83. Leroy J, Richards MW, Butcher AJ, Nieto-Rostro M, Pratt WS, Davies A, et al. Interaction via a key tryptophan in the I-II linker of N-type calcium channels is required for beta1 but not for palmitoylated beta2, implicating an additional binding site in the regulation of channel voltage-dependent properties. J Neurosci. 2005;25(30):6984–96.

84. Senkel S, Waldner C, Ryffel GU, Thomas H. Improved conditional expression systems resulting in physiological level of HNF4alpha expression confirm HNF4α induced apoptosis in the pancreatic β-cell line INS-1. BMC Res Notes. 2009;2:210.

85. Oz S, Pankonien I, Belkacemi A, Flockerzi V, Klussmann E, Haase H, et al. Protein kinase A regulates C-terminally truncated Ca$_V$1.2 in *Xenopus* oocytes: roles of N- and C-termini of the α$_{1C}$ subunit. J Physiol. 2017;595(10):3181–202.

86. Herberg FW, Taylor SS. Physiological inhibitors of the catalytic subunit of cAMP-dependent protein kinase: effect of MgATP on protein-protein interactions. Biochemistry. 1993;32(50):14015–22.

87. Eccles RL, Czajkowski MT, Barth C, Müller PM, McShane E, Grunwald S, et al. Bimodal antagonism of PKA signalling by ARHGAP36. Nat Commun. 2016;7:12963.

88. Haji-Ghassemi O, Yuchi Z, Van Petegem F. The cardiac ryanodine receptor phosphorylation hotspot embraces PKA in a phosphorylation-dependent manner. Mol Cell. 2019;75(1):39-52.e4.

89. Cheung J, Ginter C, Cassidy M, Franklin MC, Rudolph MJ, Robine N, et al. Structural insights into mis-regulation of protein kinase A in human tumors. Proc Natl Acad Sci USA. 2015;112(5):1374–9.

90. Singer-Lahat D, Lotan I, Biel M, Flockerzi V, Hofmann F, Dascal N. Cardiac calcium channels expressed in Xenopus oocytes are modulated by dephosphorylation but not by cAMP-dependent phosphorylation. Recept Channels. 1994;2(3):215–26.

91. Weiss S, Doan T, Bernstein KE, Dascal N. Modulation of cardiac Ca^{2+} channel by Gq-activating neurotransmitters reconstituted in *Xenopus* oocytes. J Biol Chem. 2004;279(13):12503–10.

92. Richard JP. Protein flexibility and stiffness enable efficient enzymatic catalysis. J Am Chem Soc. 2019;141(8):3320–31.

93. Yoo R, Haji-Ghassemi O, McFarlane C, Xu J, Petegem FV. Crystallographic, kinetic, and calorimetric investigation of PKA interactions with L-type calcium channels and Rad GTPase. bioRxiv. 2023:2023.10.24.563811.

94. Lyu L, Gao Q, Xu J, Minobe E, Zhu T, Kameyama M. A new interaction between proximal and distal C-terminus of Cav1.2 channels. J Pharmacol Sci. 2017;133(4):240–6.

95. Liu N, Yang Y, Ge L, Liu M, Colecraft HM, Liu X. Cooperative and acute inhibition by multiple C-terminal motifs of L-type Ca^{2+} channels. Elife. 2017;6.

96. Ivarsson Y, Jemth P. Affinity and specificity of motif-based protein-protein interactions. Curr Opin Struct Biol. 2019;54:26–33.

97. Masterson LR, Cheng C, Yu T, Tonelli M, Kornev A, Taylor SS, et al. Dynamics connect substrate recognition to catalysis in protein kinase A. Nat Chem Biol. 2010;6(11):821–8.

98. Zhong H, Wade SM, Woolf PJ, Linderman JJ, Traynor JR, Neubig RR. A spatial focusing model for G protein signals. Regulator of G protein signaling (RGS) protein-mediated kinetic scaffolding. J Biol Chem. 2003;278(9):7278–84.

99. Walker-Gray R, Stengel F, Gold MG. Mechanisms for restraining cAMP-dependent protein kinase revealed by subunit quantitation and cross-linking approaches. Proc Natl Acad Sci U S A. 2017;114(39):10414–9.

100. Miriyala J, Nguyen T, Yue DT, Colecraft HM. Role of Ca$_V$beta subunits, and lack of functional reserve, in protein kinase A modulation of cardiac Ca$_V$1.2 channels. Circ Res. 2008;102(7):e54-64.

101. Yang L, Katchman A, Samad T, Morrow J, Weinberg R, Marx SO. β-adrenergic regulation of the L-type Ca2+ channel does not require phosphorylation of α$_{1C}$ Ser1700. Circ Res. 2013;113(7):871–80.

102. Shistik E, Ivanina T, Blumenstein Y, Dascal N. Crucial role of N terminus in function of cardiac L-type Ca^{2+} channel and its modulation by protein kinase C. J Biol Chem. 1998;273(28):17901–9.

103. Dascal N, Lotan I. Expression of exogenous ion channels and neuro-transmitter receptors in RNA-injected *Xenopus* oocytes. In: Longstaff A, Revest P, editors. Protocols in Molecular Neurobiology. Methods in Molecular Neurobiology. 13. Totowa, NJ: Humana Press; 1992. p. 205–25.

104. Dascal N. Voltage clamp recordings from *Xenopus* oocytes. In: Rogawski M, Crawley J, editors. Current Protocols in Neuroscience. *1*. New York: John Wiley & Sons; 2000. p. 6.12.1–6..

105. Sachyani D, Dvir M, Strulovich R, Tria G, Tobelaim W, Peretz A, et al. Structural basis of a K$_V$7.1 potassium channel gating module: studies of the intracellular c-terminal domain in complex with calmodulin. Structure. 2014;22(11):1582–94.

106. Fecher-Trost C, Wissenbach U, Beck A, Schalkowsky P, Stoerger C, Doerr J, et al. The in vivo TRPV6 protein starts at a non-AUG triplet, decoded as methionine, upstream of canonical initiation at AUG. J Biol Chem. 2013;288(23):16629–44.

107. Perez-Riverol Y, Bai J, Bandla C, Garcia-Seisdedos D, Hewapathirana S, Kamatchinathan S, et al. The PRIDE database resources in 2022: a hub for mass spectrometry-based proteomics evidences. Nucleic Acids Res. 2022;50(D1):D543–52.

108. Carlson CR, Aronsen JM, Bergan-Dahl A, Moutty MC, Lunde M, Lunde PK, et al. AKAP18δ anchors and regulates CaMKII activity at phospholamban-SERCA2 and RYR. Circ Res. 2022;130(1):27–44.

109. Olsen SR, Uhler MD. Affinity purification of the C alpha and C beta isoforms of the catalytic subunit of cAMP-dependent protein kinase. J Biol Chem. 1989;264(31):18662–6.

110. Cook PF, Neville ME Jr, Vrana KE, Hartl FT, Roskoski R Jr. Adenosine cyclic 3′,5′-monophosphate dependent protein kinase: kinetic mechanism for the bovine skeletal muscle catalytic subunit. Biochemistry. 1982;21(23):5794–9.

Publisher's Note